Modelling soil erosion by water under future climate change: addressing methodological gaps

*Neil Brannigan [1] | Donal Mullan [1] | Karel Vandaele [2] | Conor Graham [1] | Jennifer McKinley [1] | John Meneely [1]

[1] Geography, School of Natural and Built Environment, Queen's University Belfast, Belfast BT7 1NN, Northern Ireland, UK.

[2] Watering van Sint-Truiden, 3800 Sint- Truiden, Limburg, Belgium.

*Corresponding author: Neil Brannigan - nbrannigan06@qub.ac.uk

Abstract

Soil erosion by water from arable land poses a serious threat to on-field agricultural productivity and the wider environment through off-site damage. Multiple studies show that climate change will worsen the impacts of soil erosion in various regions. However, these studies are limited by (1) the lack of any thorough evaluation process in applying climate scenarios to drive soil erosion models, and (2) the failure to consider the role of changing land use under future climate change, despite the evidence that it is more important than rainfall changes in driving increased erosion. Using the WEPP soil erosion model, these methodological gaps are addressed in this study for a small catchment in Belgium that is both heavily impacted by soil erosion and boasting an extensive array of mitigation measures. We develop a novel and comprehensive methodology to rigorously and efficiently select suitable climate models specifically for simulating soil erosion by water, and examine the impact of a range of environmentally and economically viable land use choices on soil erosion. The main findings reveal that our climate model selection methodology is successful in generating the widest range of likely future scenarios from a small number of models, compared with other selection methods. Our novel methodology reveals that the magnitude and frequency of soil erosion events will increase considerably under the mean of all scenarios between 2041-2100 with existing land management. Winter wheat represents the most economically and environmentally viable land use choice to effectively mitigate future soil erosion when compared to other land use alternatives under the full range of likely future climate scenarios. This research illuminates the importance of carefully tuned climate model selection and land use changes for modelling future soil erosion by water so the best- and worst-case scenarios can be adequately prepared for under a changing climate.

Key words: soil erosion; land use; climate modelling; soil erosion modelling; climate change.

1. Introduction

Soil erosion is one of the major environmental threats to arable land globally (Heitz et al., 2009; Maeda et al., 2010; Nearing et al., 2005; Panagos et al., 2015). Global soil erosion rates are estimated to be around 10.2 t ha^{-1} yr^{-1} (Yang et al., 2003), while soil renewal rates are estimated to be considerably slower at less than 0.6 t ha^{-1} yr^{-1} (Montgomery, 2007). Erosion by water accounts for the most substantial loss of soil (Panagos et al., 2015; Verstraeten et al., 2003; Yang et al., 2003), contributing to approximately 55% of global soil erosion (Bridges & Oldeman, 1999). While these soil losses pose a serious threat to on-field agricultural productivity in some places (e.g., Bakker et al., 2004; Boardman & Favis-Mortlock, 1993; Pimental et al., 1995), the most considerable damages in other places are experienced in off-site locations (Boardman, 2021; Graves et al., 2015). These impacts are most destructive where housing estates are developed next to arable farmland that is vulnerable to soil erosion by water. This kind of rural sprawl is commonplace across the European loess belt (Beckers et al., 2018), where agricultural fields are characterised by easily detachable soils. Storm events during late spring into summer cause runoff from these barely vegetated arable fields, carrying large amounts of soil as suspended sediment or bedload that induces damage to public infrastructure and freshwater systems further downstream. This phenomenon is known as 'muddy flooding' and is well-documented across several locations in Belgium (e.g., Boardman & Vandaele, 2010, 2016; Evrard et al., 2010; Evrard et al., 2007a, 2008; Mullan et al., 2016, 2019). For instance, total damages to property alone across Belgium are estimated to range from €14 million – €138 million yr^{-1}, depending on the magnitude of storm events and property value (Evrard et al., 2007b). These expenses do not include damages to public infrastructure, water quality and biodiversity, nor the costs to dredge rivers following muddy flooding events (Boardman, 2021). Muddy flooding may be regarded as a symptom of soil erosion by water, where total costs induced by water erosion globally are astronomically larger. Pimentel (2006) estimated total off-site water erosion costs of \$2.3 billion yr^{-1} for the USA alone.

Most global and regional climate models consistently project large increases in the frequency and magnitude of extreme events, while average daily rainfall intensities are also projected to rise throughout the 21st century (IPCC, 2013; Zhang, 2013). This is because temperatures are expected to increase by between 1.8°C and 4°C by the end of the 21st century (IPCC, 2013), leading to an intensified global hydrological cycle (Zhang, 2012). Extreme rainfall is highly correlated to changes in temperature, largely because of the Clausius-Clapeyron (CC) relation where the saturated vapour pressure of the atmosphere is described to increase at an approximate rate of 7% for every 1°C warming or 7% $°K^{-1}$ (Mullan et al., 2019). Furthermore, this rate is even higher for rainfall intensity

(e.g. Sun et al., 2007), with the most extreme precipitation events promoting an increase to 14% (Lenderink & Van Meijgaard, 2008). These climatic changes have caused concern that processes driven by large-scale precipitation events, such as soil erosion by water, will be exacerbated in the future (e.g. Kundzewicz et al., 2008; Nearing et al., 2005; Risbey & Entekhabi, 1996; Scholz et al., 2008; Zhang et al., 2009).

Consequently, there is a vital need to model how soil erosion and muddy flooding will be impacted by a changing climate. Comprehensive modelling is crucial for effective mitigation planning, so that vulnerable catchments will remain resilient against all possible future erosion events. While it is common to uncover studies examining future changes in soil erosion, previous modelling is limited in two main ways.

The first is the limited methodological emphasis on how climate models are selected for simulating soil erosion. It is imperative that a thorough selection process is followed to select a manageable number of representative climate models for the study application. The Coupled Model Intercomparison Project Phase 5 (CMIP5) archive (Taylor et al., 2012) contains outputs from 61 different general circulation models, such that all projections cannot be included for thoroughly studying the impacts of climate change. Constraints in computational and human resources mean that model choice must be limited to a practicable number, while an increase in the number of available models corresponds to an increase in the uncertainty remaining over future climate simulations (Lutz et al., 2016). The uncertainty provided by the spread in climate model projections is a considerable concern in climate change impact studies, commonly larger than the uncertainty associated with model parameterisation and natural variability (Finger et al., 2012; Lutz et al., 2016; Minville et al., 2008).

Secondly, modelling of future soil erosion by water rarely considers changes in land use and management. While there are some notable exceptions, (e.g., Mullan et al., 2012; O'Neal et al., 2005; Zhang & Nearing, 2005), recent research typically continues to neglect the importance of modelling the impact of future land use changes for soil erosion. Several studies reveal that land use changes are largely responsible for the increased frequency of muddy flooding events in recent years, rather than rainfall erosivity alone (e.g., Boardman & Vandaele, 2016; Butler, 2005; Olivier Evrard et al., 2007a; Verstraeten et al., 2003). Despite these findings, there remain no studies examining how land use must be managed in the future to protect off-site locations from an increased magnitude and frequency of muddy flooding events.

This study aims to address these limitations by presenting detailed and rigorous methodologies to (1) select a practicable number of climate models for subsequent soil erosion modelling, and (2)

account for future changes in land use and management. In addressing these limitations, this study represents an advance from previous research modelling soil erosion by water. The selected study area is a heavily impacted and mitigated catchment in Belgium. The wider benefits of this research include facilitating adequate mitigation planning for this catchment under a changing climate, while also demonstrating the importance of carefully selecting climate models and accounting for changes in land use in modelling soil erosion by water in other regions.

2. Material and Methods

2.1. Study Area

While muddy floods are commonly reported in several locations across the European loess belt – such as the South Downs in the UK, South Limburg in the Netherlands, Northern France, and parts of Slovakia (Boardman et al., 1994) – these events are most widespread in Belgium (Evrard et al., 2007a). Previous research (Evrard et al., 2007a) found that 68% of all municipalities across the Belgian loess belt have been affected by muddy flooding in the past. The Belgian loess belt (Figure 1) is an 8867 km^2 plateau that gently slopes north with a mean altitude of 115 m. Belgium has a temperate maritime climate with mild winters and cool summers, influenced by the North Sea and Atlantic Ocean. As determined from the E-OBS high-resolution (0.25°) gridded dataset over Europe (Haylock et al., 2008) between 1981 and 2010, mean annual temperatures ranged from 3°C in January to 18°C in July and August for the grid square containing the study area (https://climexp.knmi.nl/). Rainfall has a relatively even distribution throughout the year, with average annual rainfall amounts ranging from 520 mm to 960 mm in the study area (~ 55 mm to 75 mm per month). The Belgian loess belt possesses the highest density of cultivated land in the country (Beckers et al., 2018). Summer crops – such as maize, potatoes, and sugar beet – have increased in recent decades and now dominate the arable land in place of winter cereals. Cover crops such as mustard and phacelia are often encouraged to shield the soil during late spring and early summer while summer crops reach maturity (Bielders et al., 2003; Mullan et al., 2016).

This research focuses on a dry valley locally known as the 'Heulen Gracht' (50.76° N, 5.12° E) located within the 200 km^2 Melsterbeek catchment in the Limburg province of Belgium. The Heulen Gracht is a prominent landscape for academic and community research on muddy flooding problems and solutions (e.g., Boardman & Vandaele, 2020; Evrard et al., 2007b, 2008), covering a 3 km^2 area. The study area drains into Velm Village, which has a local reputation as a 'devastated village' after

repeated flooding in recent decades. Mitigation measures were first installed in 2002 to remain resilient for a 20-year period, with each illustrated in Figure 2. Mitigation includes several grass buffer strips (GBS) to trap sediment on-site, a ~430 m grassed waterway (GWW) along the catchment thalweg to prevent ephemeral gullying, along with detention ponds and earth dams that together act to reduce peak discharges by buffering runoff. Renewed mitigation planning is urgently needed so the catchment remains resilient to future climatic pressures for the next 20 years and beyond, where intensified storm conditions are expected to cause an increase in the frequency and magnitude of erosion events (Mullan et al., 2019).

This study focuses on the downstream half of the Heulen Gracht (approximately 1.3 km^2) to allow for high-resolution drone imagery, such that an altitude of between 107 and 140 metres (m) was determined (Figure 3). Drone imagery gathered in December 2019 revealed that cropland covers 73% of the catchment surface, grassland 8%, woodland and hedgerows 2%, orchards 16%, and roads (1%) account for the remainder. A singular hillslope that feeds into the GWW-mitigated catchment thalweg was selected for explicit analysis, such that this hillslope will hereby be referred to as the 'GWW Hillslope.' This hillslope was chosen because it directly contributes to sediment output observed at the catchment outlet (Figure 2). A separate hillslope – henceforth referred to as the 'GBS Hillslope' – was also selected to support model validation at a later stage. While this hillslope is located next to the catchment outlet, a 21 m wide GBS at the foot of the hillslope considerably reduces sediment contribution to the catchment thalweg (Figure 2). It is for this reason that the GBS Hillslope was not chosen for soil erosion-climate change analysis at a later stage – unlike the GWW Hillslope, extensive mitigation at the GBS Hillslope means that the impacts of future changes in climatic conditions on soil erosion and muddy flooding at the Heulen Gracht will not be clearly demonstrated. Key geomorphological characteristics for both hillslopes are described in Table 1. Soil erosion at both hillslopes was simulated under baseline conditions as described below for model validation purposes, while the impacts of future changes in climatic conditions and land use on soil erosion are analysed explicitly for the GWW Hillslope alone.

2.2. Baseline Soil Erosion Modelling

The Water Erosion Prediction Project (WEPP) model (Flanagan & Nearing, 1995; v.2012.8) is applied to fulfil the objectives of this study. WEPP is a spatially-distributed continuous simulation model, providing long-term simulations of soil erosion and deposition along with other key soil, hydrology, and plant components at hillslope, field and small catchment (< 260 ha) scales (Laflen et al., 1991;

Ascough et al., 1995; Li et al., 2017). WEPP can predict soil erosion, sediment transport, and deposition across the landscape by applying a steady-state continuity equation to predict rill and inter-rill erosion processes. WEPP is widely applied within climate change-soil erosion research, with success demonstrated in a range of studies (e.g. Mullan et al., 2016; Stolpe, 2005), not least to investigate muddy flooding for a hillslope in the Melsterbeek catchment in Mullan et al. (2016, 2019). The following sections describe the datasets and methods used to drive WEPP for use in this study.

2.2.1. Soil

A 0.3 m deep bulk soil sample was taken every 10 m at both hillslopes using a soil auger (Appendix A), reaching a maximum depth of 1.8 m. Table 1 reveals that lab analysis of topsoil (0.3 m) textures at both the GWW and GBS Hillslopes using a Malvern laser granulometer is consistent with previous topsoil sampling for the Heulen Gracht and other analogous catchments in the Belgian loess belt recorded in Evrard (2008). Average organic matter (OM) content presented in Table 1 was found using a Loss on Ignition (LoI) approach, where soil samples were placed in a furnace at 450°C. As before, topsoil OM measured at the GWW Hillslope is consistent with an analogous catchment < 15 km from the study area (Mullan et al., 2016, 2019), while slightly higher topsoil OM at the GBS Hillslope owes to > 30% grass coverage along the hillslope. Soil depths between 0.6 m and 1.8 m were collected at the GBS Hillslope to represent soil characteristics at both the GBS and GWW Hillslopes. Critical shear, hydraulic conductivity, and rill and interrill erodibility values were estimated by WEPP based on equations given in the WEPP user manual (Flanagan & Livingston, 1995). These equations were derived from data collected at several WEPP erodibility sites in the USA under a rainfall simulator. These values are important in determining soil detachment and other erosion processes, but practical constraints in obtaining field measurements meant estimates had to be made. Encouragingly, these estimated values were found to perform well against measured values for several WEPP erodibility sites in the USA, with close model fits for all erodibility parameters (Alberts et al., 1995). Values are representative of the entire hillslope and are dependent on soil parameters such as particle size – which was measured in the laboratory in this study. The estimated WEPP values therefore rely on some field measured data specific to the study location. Estimated albedo was set at 0.1, CEC (meq/100g) at 15, and initial soil saturation at 75% for each hillslope – these values were derived from a WEPP soil input file for a neighbouring hillslope as outlined in Mullan et al. (2016; 2019).

2.2.2. Slope

Slope profiles were established for both hillslopes following a high-resolution drone survey[1] (necessary for a wider project outside the remit of this paper) with an average ground sampling distance (GSD) of 2.3 cm. Sampling distance was increased to 6 m in keeping with WEPP input value limitations. This was achieved by averaging all slope values within a 6 m distance. While 2 cm resolution provides a slope profile that is very closely representative of the true slope profile, WEPP is incapable of processing slope data of this resolution for greater than 2 m distance downslope. WEPP allows up to 100 data points for both cumulative distance (ft) and slope (%), respectively, yet input value totals ≥ 50 tend to generate a distorted slope profile that produces unreasonable soil erosion values.

2.2.3. Land Management

Land use data between 2008 and 2018 were collected from Geopunt Vlaanderen (https://www.geopunt.be/kaart), which is an open source database provided by the Flemish Government. Crop rotation dates were sourced by the local soil erosion expert, Dr Karel Vandaele. Information concerning temperature (base, optimal, and maximum) and leaf area index for crops in Belgium were sourced from Gobin (2010, 2012). All remaining plant growth parameters were calculated by WEPP for each crop without additional modifications (Flanagan and Nearing, 1995). Land management details required to simulate WEPP for the GWW Hillslope are displayed in Appendix B. Land management details required to validate WEPP simulations at the GBS and GWW Hillslopes are shown in Appendix C.

2.2.4. Climate

Baseline climate data were simulated using the stochastic weather generator CLIGEN (Nicks et al., 1995), which draws on the statistical properties of observed climate measurements to generate long-term daily climate data. All required CLIGEN input parameters are presented in Table 2. Previous studies (e.g. Nearing et al., 1990) have demonstrated that precipitation variables provide

[1] A Class 1 Phantom 4 RTK drone was flown 91 m above the ground surface at 3.5 m/s, using a single grid with 80/80 overlap. The flight required seven high-capacity battery packs.

the greatest influence on soil loss and runoff projections using WEPP. Mean precipitation per wet day is calculated using monthly means, skewness, and standard deviation values. Series of wet and dry days are determined from the transitional probabilities of a wet day following a wet day (Pw/w) and a wet day following a dry day (Pw/d). Rainfall intensity is calculated from determinations of monthly half hour precipitation (MX.5P) and time to peak storm intensity (Time PK). Time PK is a dimensionless variable that represents an empirical probability distribution of the time to peak storm intensity as a fraction of storm duration, such that this is the only variable that is not calculated for each given month (Mullan et al., 2019; Yu, 2003).

High resolution (0.25°) observed (E-OBS) daily temperature and precipitation data from 1950-2019 (Haylock et al., 2008) were downloaded from the Royal Netherlands Meteorological Institute (KNMI) Climate Explorer site (http://climexp.knmi.nl) for the grid containing the study area. The Niel-bij-Sint-Truiden climate station (pinned in Figure 1, less than 3 km from the Heulen Gracht) provided sub-hourly precipitation data between 2004 and 2014 to determine Time Pk and MX.5P. The remaining parameters – solar radiation, wind speed and direction, and relative humidity – were sourced from nearby Maastricht, Netherlands. Equation 1 was used to convert relative humidity to dew point temperature (Alduchov & Eskridge, 1996). CLIGEN simulations were conducted for 330 years to represent 30 cycles of each 11-year crop rotation in WEPP, as recommended by Mullan et al. (2019).

$$TD = \frac{243.04\left(LN\left(\frac{RH}{100}\right) + \frac{(17.625 * T)}{(243.04 + T)}\right)}{\left(17.625 - LN\left(\frac{RH}{100}\right) - \frac{(17.625 * T)}{(243.04 + T)}\right)} \quad (1)$$

where TD = dew point temperature (°F); LN = natural logarithm; RH = relative humidity (%); and T = mean temperature (°F).

2.2.5. Model Validation

Despite considerable research focus attributed to the study area in recent years (e.g., Boardman & Vandaele, 2020; Evrard et al., 2008), no hillslope specific soil loss information was previously gathered. We have, however, made use of previously calculated (Evrard, 2008) mean annual specific sediment yield (SY) at the outlet of the catchment, which measured 0.5 t/ha between 2006 and 2007. This SY data remains the only suitable measured data at the catchment to validate simulations

of mean annual SY using WEPP. Two separate hillslopes – the GWW and GBS Hillslopes – that directly contribute to SY at the catchment outlet were selected to adequately validate the soil erosion model for the study area against these previous measurements under 2006-2007 climate and land use. In accordance with ortho-imagery collected between 2006 and 2007, the GBS Hillslope was simulated under winter wheat for both years, while winter wheat was rotated with sugar beet for the GWW Hillslope. WEPP simulations were carried out in watershed mode since both hillslopes feed into the same drainage channel. While other hillslopes may also contribute to sediment output at the catchment outlet, the GWW and GBS Hillslopes were largely chosen based on field access in June 2019. Expansive areas of dense cover crops limited field access to other hillslopes (Figure 2).

2.3. Climate Model Selection

It is routine in previous climate change-soil erosion studies to select a small subset of climate models for impact analysis, yet the reasons for selecting specific models are often arbitrary or justified based on some simple statistical information relating to the models. We compare three different approaches in this study for the GWW Hillslope, outlined below in Sections 2.3.1-2.3.3. The selection method that yields the widest range in projections for key soil erosion and muddy flooding diagnostics (while using an equal number of climate scenarios) during 2081-2100 climatic conditions will be determined the most desirable method for climate model selection. It is anticipated that the discrepancy in climatic conditions represented by each climate model will be most apparent for a distant future period. While near future (2021-2040) and mid-future (2041-2060 and 2061-2080) climatic conditions are examined at a later stage for the GWW Hillslope using the subset of selected climate models, time constraints mean that evaluating climate models for each of these time steps under each climate model selection method is highly impractical. Although a wide envelope of uncertainty makes adaptation and planning decisions difficult, it is important to capture the widest spread of likely climate scenarios to account for a wide array of potential climate futures – without the need to apply dozens of climate models to soil erosion impact studies. It is important to emphasise that this novel targeted methodology includes an analysis of climate model skill, such that this wide range of uncertainty is reasonably reduced by only selecting climate models that display sufficient skill in simulating the present-day climate for the study area.

2.3.1. Past-Performance and Envelope (PPE) Method

While climate models are commonly chosen based upon their past-performance (e.g., Biemans et al., 2013; Pierce et al., 2009) – i.e., their ability to closely simulate present and near-past climate – it is plausible that potential climate scenarios may be omitted. Alternatively, the 'envelope approach' ensures that a broad range of projections for a given climatological variable is represented from a selected ensemble of models. However, by neglecting the skill provided by the model in simulating present and near-past climate, this approach assumes that all models are equally plausible. With these limitations in mind, the revised methodology applied in this research (herein referred to as the PPE method) is inspired by the concept provided in Lutz et al. (2016) to combine the past-performance and envelope approaches for selecting a manageable number of the most suitable climate models. PPE adapts and departs from the envelope approach in Lutz et al. (2016) to be specifically applicable to precipitation-driven phenomena, while certain key precipitation characteristics necessary to run CLIGEN in WEPP are compared to assess model past-performance.

Precipitation data (mm/day) from each model were downloaded for both a moderate radiative forcing scenario – representative concentration pathway (RCP4.5) – and a high radiative forcing scenario – RCP (RCP8.5) for the future period (2081-2100), with E-OBS 1950 – now 0.25° Europe observed data (1986-2005) used as a historical baseline. The average ΔP between the future period and the observed period was calculated for all models for both RCP4.5 and 8.5. RCP4.5 provided 102 model runs, while RCP8.5 provided 77 model runs. All available initial condition ensemble members were included for all models since each initial condition ensemble member leads to a different future. To avoid selecting outliers, the 10th and 90th percentile values for ΔP for both RCPs were determined. These percentile values represented 'wet' (90th percentile) and 'dry' (10th percentile) sides. All models, irrespective of time step scale, were added to the initial selection of models to calculate the percentile values, thereby ensuring that all projected possible scenarios were fully represented. The three daily time step models with the lowest distance from each side were selected by subtracting the precipitation value (mm/day) from each percentile value. The selected wet and dry models for RCP4.5 and RCP 8.5 are provided in Table 3.

Lastly, the skill of each of the remaining models was evaluated through a past-performance analysis. The purpose of this step was to further narrow down model choice to models that most closely simulate observed metrics of precipitation that are important for muddy flooding. Certain precipitation characteristics necessary to run CLIGEN in WEPP were compared between observed and historical modelled data for the selected models, shown in Table 3. These precipitation characteristics were normalised by expressing each variable as a fraction of the maximum modelled value for each given variable, such that each precipitation characteristic was granted equal weight. Any negative values were converted to positive. Table 4 ranks the model performance, with first

rank corresponding to least difference. The three models with the least difference in values for each RCP were selected, with the final selected models provided in Table 5. HADGEM2-AO (Table 3) was excluded from this step since we lacked the necessary computer memory to extract data for this model. This past-performance analysis ensured that the final model range represented all likely future scenarios, rather than simply generating the widest range of all CMIP5 projections.

2.3.2. Equilibrium Climate Sensitivity (ECS) Method

Selecting climate models based on the range of highest and lowest ECS values provided by the IPCC (Kattsov et al., 2013) is popular in soil erosion research (e.g. Mullan et al., 2016, 2019). ECS considers changes in water vapour, clouds, lapse rate, and surface albedo to calculate warming for a doubling of atmospheric CO_2 compared to preindustrial climate once a new climatic equilibrium is achieved. Accordingly, ECS has been used to describe the severity of future climatic changes (Knutti *et al.*, 2017).

In keeping with the criteria applied for PPE, ECS values below the 10^{th} percentile and above the 90^{th} percentile of all ECS values for the CMIP5 models were excluded. The three models nearest to the 10^{th} percentile and the three models nearest to the 90^{th} percentile were selected. Models nearest to the 10^{th} percentile were simulated under RCP4.5, while the models nearest to the 90^{th} percentile were simulated under RCP8.5. The selected ECS models are displayed in Table 5.

2.3.3. Random Selection (RS) Method

Previous climate change impact studies have also included CMIP5 models with little to no justification of selection (e.g. Fazeli Farsani et al., 2019; Sardari et al., 2019; Sha et al., 2019). Consequently, three iterations of random model selection (herein referred to as RS) were used to determine whether different combinations of models selected at random could provide a wider range in soil erosion and muddy flooding diagnostics compared to the carefully tuned methodological approaches applied for PPE and ECS. Of course, a wider range in projections provided by RS would be simply by chance and it would not consider past performance, unlike PPE. The RS models were separated into three groups in Table 5 – Random Group 1 (RG1), Random Group 2 (RG2) and Random Group 3 (RG3) – randomly assigned as RCP4.5 or RCP8.5.

2.4. Spatial Downscaling

Climate information for each model from the *Earth System Grid Federation* (ESGF) (https://esgf-node.llnl.gov/search/esgf-llnl/) is provided at the grid box scale of each climate model. These models aim to represent the full Earth system and use RCP scenarios to produce projections of future climate (Hawkins et al., 2013). Spatial downscaling is required to reduce the grid box scale to match the observed climate dimensions and this has been applied to all models (Table 5). The original grid box scale for each model is provided in Appendix D.

Observed precipitation (1986-2005) was plotted against the ranked quantiles of the reference period (1986-2005) for the selected models on a monthly basis using QQ-plots (e.g., Mullan et al., 2019). Polynomial functions were applied to the precipitation data for each model, and appropriate ordering (mostly third order) was applied to each model to avoid clearly anomalous precipitation data points. Alternatively, observed TMAX and TMIN were calibrated using the change factor (CF) approach, as outlined in Hawkins *et al.* (2013). The CF method (Equation 2) changes the simulated modelled output of mean and daily variance by using the observed daily variability (Arnell et al., 2003; Gosling et al., 2009). This method was previously found to be more robust than those using model variability, such as the bias correction method (Hawkins et al., 2013). While the CF approach is widely accepted for calibrating temperature data, the positive definite nature of precipitation makes calibration more complex (Hawkins et al., 2013).

$$T_{CF}(t) = \overline{T_{RAW}} + \frac{\sigma_{T,RAW}}{\sigma_{T,REF}} \left(O_{REF}(t) - \overline{T_{REF}}\right), \qquad (2)$$

where $T_{CF}(t)$ is the change factor for temperature (°F); $\overline{T_{RAW}}$ is the raw modelled temperature for a future period and $\overline{T_{REF}}$ is the observed, where the bar above the symbol represents the time mean; $\sigma_{T,RAW}$ indicates the standard deviation (°F) of the daily raw model output for the future period and $\sigma_{T,REF}$ indicates the standard deviation of the daily model output for the reference period ; O_{REF} indicates the daily observations.

2.5. Temporal Downscaling

Temporal downscaling is also required to generate daily scenarios from monthly scenarios, which is necessary to perturb CLIGEN within WEPP. Raw historical (1986-2005) and future (2021-2100) precipitation data from the selected models were temporally downscaled to produce daily scenarios.

While 2081-2100 was selected to contrast each model selection method, future changes in soil erosion were later examined between 2021 and 2100 using the most desirable model selection method. Raw TMAX and TMIN data for the historical and future periods were also downscaled to produce daily scenarios, as needed for WEPP simulations.

Transitional probabilities (Pw/w and Pw/d) were determined by categorising historical precipitation into wet months, dry months, and all months. Wet months were defined when monthly precipitation totals equalled or exceeded the 90th percentile of the mean monthly precipitation totals for each respective month during the reference period (1986-2005). Dry months were defined when monthly precipitation totals did not meet this percentile value. Linear relationships were established between historical monthly precipitation totals and the transitional probabilities for wet months, dry months, and all months. These transfer functions were forced with future monthly precipitation totals to calculate future transitional probabilities. Mean P was calculated following the method in Zhang et al. (2004). Equation 3 was applied to calculate the unconditional probability of precipitation occurrence (π):

$$\Pi = \frac{P\ w/d}{1 + P\ w/d - P\ w/w} \quad (3)$$

the new $Mean\ P$ was then calculated using Equation 4:

$$Mean\ P = \frac{R_m}{N_d \pi} \quad (4)$$

where $Mean\ P$ (in) was described previously, R_m is the projected mean precipitation totals (in) for a given month, and $N_d\pi$ is the expected number of wet days in the month.

Table 6 is adapted from Mullan et al. (2019) to detail how the CLIGEN parameters were adjusted to represent future climate changes. Aside from Mean P, P(W/W), P(W/D), AV TMAX, and AV TMIN, all remaining CLIGEN parameter monthly values were calculated by developing linear relationships using the historical data (1986-2005). A summary of all steps described for each model selection method is provided in Figure 4.

2.6. Land Management Changes

Several previous studies anticipated how climate change will impact farmer crop management in the future across the Belgian loam belt (e.g., De Frutos Cachorro et al., 2018; Gobin, 2010, 2012). A range of likely future land management scenarios was developed as part of a 'what-if' scenarios

approach (e.g., Mullan, 2013; Mullan et al., 2012) using this previous research, as seen in Figure 5. These scenarios are informed by economic and environmental biases (Mullan, 2013), while a scenario that pulls together both of these biases is also considered with several sub-scenarios to improve predictive capability. This latter scenario approaches winter wheat as a highly profitable asset in the future when compared to common summer crops. Winter wheat shows considerably less vulnerability to adverse weather conditions associated with climate change (Gobin, 2018) – such as heat and drought stress – when compared to summer crops. Unlike winter wheat, summer crops will require increased irrigation and other highly expensive management practices (De Frutos Cachorro et al., 2018). Winter wheat also offers increased soil protection when compared to summer crops. Consequently, winter wheat only is planted in the first sub-scenario, while the second sub-scenario involves the addition of a cover crop that is planted in late August following harvesting. The final sub-scenario indicates land use remaining the same as the present-day, where winter wheat is rotated with summer crops.

A purely economic scenario involves only summer crops being planted. It is possible that summer crops will remain profitable in the future if the prices of summer crops continue to increase (De Frutos Cachorro et al., 2018), such that the additional costs to manage summer crops under future climatic conditions will be insubstantial. Lastly, a return to grassland represents an extreme environmental scenario, such that government and business strategies will be heavily influenced by increased environmental awareness at local and national scales. Planting and harvesting dates for all crops under each respective scenario will also remain unchanged in the future. While it is possible that climatic changes will correspond to changing planting and harvesting dates in the future, this is a complex consideration to simulate that requires calculating several climatological variables and it is beyond the scope of this study. In saying this, Gobin (2018) reveals that farmers have previously not adjusted sowing dates despite warmer temperatures in Belgium.

3. Results

3.1. Model Validation

The sum of modelled SY contributed by the GWW and GBS Hillslopes reveals an underestimate by just 0.3 t/ha from measurements at the catchment outlet in Evrard (2008). The GWW Hillslope accounts for almost all SY contributed towards the catchment outlet (Appendix E) between 2006 and 2007, while all remaining SY is generated by channel erosion. The GBS Hillslope does not contribute

any SY for these years, owing to winter wheat coverage during both years and the 21 m GBS at the foot of the hillslope that acts to trap sediment. This slight underestimation in mean annual SY is to be expected considering that two hillslopes alone cannot account for all sediment contributions towards the catchment outlet, as implied in Figure 3. Other unmitigated hillslopes not considered here also feed into the drainage channel (Figures 2 and 3). In this respect, it appears that WEPP has closely simulated mean annual SY to measurements in Evrard (2008) at the catchment outlet between 2006 and 2007.

3.2. Comparing Model Selection Methods

Figure 6 demonstrates that PPE provides the widest range in mean annual precipitation response projected at the GWW Hillslope from six separate CMIP5 models, with 'dry' and 'wet' models determining the soil erosion and muddy flooding response. PPE consistently projects a wider spread in future scenarios compared to ECS. The ranges (highest minus lowest model value) in SY and SL projected by PPE are 168% and 80%, respectively, higher than ECS. PPE projects an increase in runoff by 130% compared to ECS. RG1 and RG2 projections are marginally closer to PPE. The range in PPE SY is higher than RG1 and RG2 by 26% and 37%, respectively (Figure 6). Differences in SL projections between both methods closely reflect differences in SY observations, while PPE also generates the widest model spread for runoff.

Return period analysis is important for examining future changes in the frequency and magnitude of events. Return period intervals of 2, 5, 10, 20, 25, 50 and 100 years are displayed for each model selection method in Table 7. As seen for the mean annual projections (Figure 7), Table 7 reveals that PPE consistently generates the widest model response for SY. Differences in projections between each selection method are most clearly represented at a 1 in 100-year event. The range for PPE SY is higher than ECS, RG1, RG2, and RG3 by 8 t/ha, 9.6 t/ha, 22.2 t/ha, and 2.9 t/ha, respectively, for a 1 in 100-year event. Table 7 reveals that RG2 generates the widest response in daily precipitation for all return period intervals, closely followed by PPE. The widest difference between these methods is observed for a 1 in 50-year event, where daily precipitation for RG2 exceeds PPE by 11.1 mm. ECS consistently projects the lowest range in daily precipitation for all return periods.

3.3. Climate Change Impacts

3.3.1. Mean Annual Changes

Figure 7 reveals that mean annual SY at the GWW Hillslope is projected to increase by 392% (+ 3.3 t/ha) from the baseline to 2081-2100, while mean annual soil loss (SL) between 2081 and 2100 represents an increase from the baseline of 409% (+ 0.83 kg/m^2). Similarly, mean annual runoff depth increases from the baseline by 269% (+ 8.41 mm) between 2081 and 2100.

Marginal mean annual changes from the baseline are observed for the 2021–2040 period (Figure 7). Mean annual SY and SL during 2021–2040 increase from the baseline by 0.26 t/ha (30%) and 0.1 kg/m^2 (51%), respectively, while mean annual runoff depth increases by 1.07 mm (35%). Considerable increases for these key diagnostics begin from 2041–2060. Mean annual SY increases during 2041-2060 by 92% (+ 1.02 t/ha) compared to 2021-2040, while mean annual SL increases by 70% (+ 0.21 kg/m^2) and mean annual runoff depth increases by 55% (+ 2.32 mm) for the same period. Interestingly, the 2061-2080 period represents a decline in mean annual SY (- 0.11 t/ha or–-5%) when compared to 2041 and 2060, while mean annual SL decreases by 0.05 kg/m^2 (- 9%) and mean annual runoff depth marginally increases (+ 0.46 mm or + 7%). Mean annual SY, SL and runoff continue to increase considerably between 2061-2080 and 2081-2100 with increases of 107% (+ 2.2 t/ha), 84% (+ 0.47 kg/m^2) and 62% (+ 4.44 mm), respectively. Noticeably, the range in model projections increases over time from 2021-2040 and 2081-2100 as the magnitude of mean annual SY, SL and runoff increase.

3.3.2. Seasonal Changes

Baseline SY at the GWW Hillslope clearly demonstrates a muddy flooding season that begins in May or June and ends in September with a clear peak in SY observed in August, as displayed in Figure 8. It is immediately apparent that an earlier and longer muddy flooding season is projected in the future between 2021 and 2100. Figure 8 reveals that SY begins to rise in May and declines in December. June represents the peak month of SY during 2021 and 2040, with smaller spikes observed in August and November. Similar seasonal changes in SY are observed between 2041 and 2060, except the peak month for SY is noticeably projected during August. SY during 2061-2100 also reaches its peak in August. Unlike during 2021-2040, peak seasonal SY during 2041-2100 surpasses the baseline peak SY (Figure 8).

3.3.3. Return Periods

Figure 9 illustrates the mean and maximum of all modelled return periods for SY and precipitation at the GWW Hillslope, which reveal distinct differences between the baseline and future time series.

The maximum of all modelled return periods reveals that the frequency of high magnitude events is projected to increase along with the magnitude of SY between 2021 and 2100 (Figure 9). SY projections between 2021 and 2100 are consistently higher than the baseline for all return periods. The 2081-2100 period displays the most considerable increases in SY from the baseline for all return periods. For instance, a 1 in 10-year event for SY during 2081-2100 represents an increase from baseline SY for a 1 in 100-year event of 3.8 t/ha. Alternatively, the mean of all modelled return periods reveals that baseline climatic conditions generate a higher magnitude event for the maximum return period compared to 2021-2040 projections (Figure 9). Baseline SY for a 1 in 100-year event represents an increase from 2021-2040 SY by 3.3 t/ha for the same return period. Otherwise, 2041-2100 projections of mean SY are consistently higher than the baseline for all return periods (Figure 9).

The magnitude of maximum and mean daily precipitation is consistently higher than the baseline, and these increases typically become more prominent as time progresses for each return period. A notable exception is observed for 2041-2060 and 2061-2080 daily precipitation. Mean daily precipitation is consistently higher during 2041-2060 compared to 2061-2080 for all return periods, while maximum daily precipitation for a 1 in 50-year event is higher by 7.2 mm during 2041-2060 compared to 2061-2080 (Figure 9).

3.4. Land Use Impacts

3.4.1. Mean Annual Changes

Figures 10-12 demonstrate that alternative land management practices considerably impact projections of SY, SL and runoff at the GWW Hillslope between 2021 and 2100. However, it is still apparent for all land use scenarios that each of the modelled diagnostics displays an increase in magnitude over time. Noticeably, a broader range in model projections for each land use scenario is reflective of a higher mean modelled magnitude of soil erosion.

Mean annual SY projections between 2021 and 2100 reveal that only planting summer crops induces the most soil erosion of all land use scenarios (Figure 10). Mean annual SY under the summer crops

scenario represents an increase from the baseline by 14% (0.15 t/ha) between 2021 and 2040, 2% (0.05 t/ha) between 2041 and 2060, 0.3% (1.11 t/ha) between 2061 and 2080, and 5% (0.22 t/ha) between 2081 and 2100. While the baseline scenario represents a slight decrease from summer crops only, current land management consistently generates higher mean annual SY than for all remaining land use scenarios. The baseline scenario projects higher mean annual SY than the winter wheat with cover crop scenario by 0.82 t/ha between 2021 and 2040, 1.2 t/ha between 2041 and 2060, 1.2 t/ha between 2061 and 2080, and 2.6 t/ha between 2081 and 2100. While the winter wheat with cover crop scenario represents a 0.29 t/ha decrease in mean annual SY from the winter wheat only scenario between 2061 and 2080, the latter typically projects slightly lower mean annual SY than the former. The winter wheat with cover crop scenario projects higher mean annual SY by 0.08 t/ha between 2021 and 2040, 0.37 t/ha between 2041 and 2060, and 0.62 t/ha between 2081 and 2100 when compared to the winter wheat only scenario (Figure 10). The grass scenario projects very low mean annual SY between 2021 and 2100, such that the values are barely represented in Figure 10. Figure 11 reveals similar observations for mean annual SL.

Figure 12 demonstrates that the baseline generates the highest mean annual runoff depth of all land use scenarios. Mean annual runoff depth represents an increase from the only planting summer crops by 0.37 mm between 2021 and 2040, 0.95 mm between 2041 and 2060, 0.89 mm between 2061 and 2080, and 1.4 mm between 2081 and 2100. Besides grassland during 2021-2040 where mean annual SY is lower than for only planting summer crops by just 0.43 t/ha, all remaining scenarios show noticeable decreases in mean annual runoff depth compared to planting summer crops only. However, each of these remaining land use scenarios projects similar mean annual runoff depth changes within the range of 1.62 mm between 2041 and 2060 and 1.05 mm between 2061 and 2080 The range in mean annual runoff depth increases to 5.7 mm during 2081-2100 between grassland, winter wheat only, and winter wheat with cover crop scenarios. Unlike for mean annual SY and SL, grass generates a sufficiently high mean annual runoff depth response that is easily identifiable in Figure 12.

3.4.2. Seasonal Changes

Land use choice also influences the seasonal distribution of peak SY between 2021 and 2100. This is well represented in Figures 13-15 for the winter wheat only, winter wheat with cover crop, and summer crops only scenarios, respectively, at the GWW Hillslope. Seasonal changes for the grass scenario are omitted, since SY remains very low between 2021 and 2100.

Land management without summer crops clearly offers a shorter muddy flooding season between 2021 and 2100 (Figures 13 and 14). Only planting winter wheat or winter wheat with a cover crop typically generates one defined peak in SY that displays a rise and fall within three months or shorter. An exception is observed for winter wheat with cover crops during 2021-2040 where February presents a slight peak in SY, and a rise in SY is shown in January in 2061-2080 (Figure 14). While October and December are the peak months of SY during 2061-2080 for winter wheat only, peak SY is otherwise observed in November up to 2100 (Figure 13). Planting a cover crop with winter wheat typically causes future peak SY to be observed September, except for 2021-2040 where November represents the peak month of SY (Figure 14). Only planting summer crops offers similar seasonal patterns of SY when compared to the baseline scenario where land use remains the same as the present day (Figure 15).

4. Discussion

4.1. Importance of PPE Selection

As shown in Figure 6 and Table 7, selecting climate models based on most increased wetness and least increased wetness distinctly provides a broader range in projected soil erosion diagnostics compared to selecting models based on highest and lowest ECS values. PPE also largely demonstrates a wider spread in projections compared to almost all random scenarios, with only minor exceptions. To this end, PPE is successful in generating the widest range of sensible future scenarios, which has not been achieved elsewhere for modelling soil erosion by water.

The range in PPE results is said to be 'sensible' because the skill of each model was also assessed by only selecting models that closely simulate relevant metrics of precipitation to observations, while model outliers were removed using the 10^{th} and 90^{th} percentile of all delta changes as part of the envelope selection (Section 2.3.1). PPE generates a model range that captures all likely future scenarios. ECS and random selection fail to consider the skill of each model, while also commonly generating a narrow spread in model projections such that possible futures may be omitted.

4.2. Future Mean Annual Changes in Soil Erosion

Consistent with findings in Mullan et al. (2016, 2019) for an analogous catchment in Flanders, the magnitude of soil erosion and muddy flooding in the Heulen Gracht is clearly projected to increase in the future and the frequency of high magnitude events will also increase considerably. These increases noticeably become more prominent as time progresses under both mean and maximum modelled return periods. Mean annual modelled projections of SY, SL and runoff during the 2081-2100 period certainly reveal drastic increases in the magnitude of erosion when compared to baseline observations. While the 2061- 2080 period represents a slight decrease from 2041-2060, increases in the magnitude of erosion from the baseline remain substantial. Under current land management practices, results in Figures 7-9 strongly suggest that existing mitigation measures for the study area must be adapted to remain effective under future climatic conditions. This is unless land management is adjusted in keeping with the grassland and winter wheat practices displayed in Figures 10-12, where each of these scenarios generates a reduced soil erosion response under each future time slice when compared to observations (1986-2005) under current climatic conditions and land management practices.

It is highly likely that economic biases will continue to influence future crop rotations at the study area. Planting just summer crops represents the most aggressive economic approach under the circumstance that the prices of summer crops increase in the future. However, this scenario clearly demonstrates an increased soil erosion threat when compared to current conditions (Figure 15). This increased soil erosion response is due to reduced soil cover, such that the soil surface is highly vulnerable to intense precipitation events in late spring and early summer. Increased exposure of the soil surface thereby facilitates soil detachment, while a soil surface crust can develop that reduces infiltration rates and increases runoff generation (Evrard et al., 2008). On the other hand, conversion to grassland represents the most environmentally conscious option but perhaps the least likely scenario to be accepted by farmers in the future given the severe economic drawbacks. While minimal SY and SL is consistently projected between 2021 and 2100 for grassland, this scenario offers a similar runoff resistance to winter wheat only and the winter wheat with cover crop scenarios. These runoff observations are consistent with findings in Evrard (2008) for the Heulen Gracht. Runoff coefficients differ by only 0.01 between grassland and dense cropland such as winter wheat, while runoff velocities of 0.1 m/s^{-1} are shared between both land use types (Evrard, 2008).

Alternatively, Figures 10-12 reveal that winter wheat will be highly effective in offering off-site protection from soil erosion in the future, while also being recognised as an economic asset under a changing climate where heat and drought stress will become increasingly prevalent (De Frutos Cachorro et al., 2018). Winter wheat generates a reduced soil erosion response because of increased soil surface cover that prevents considerable soil detachment during high intensity rainfall events.

This is unless winter wheat continues to be rotated with a selection of summer crops, as observed currently. Existing land management practices appear to effectively manage soil erosion together with mitigation measures under current climatic conditions, but mean modelled projections of soil erosion between 2041 and 2100 reveal considerable increases that will pose an increased risk to nearby off-site locations (Figure 7). It also appears to be unreasonable to plant a cover crop alongside winter wheat. Despite the increased canopy coverage provided by the cover crop that acts to protect the soil surface from rill erosion (Phai et al., 2006; Valentin et al., 2005), the additional tillage practice required to manage the cover crop increases soil vulnerability and thereby erosion. Tillage practices reduce soil roughness (Corbane et al., 2008), such that tillage erosion is at least as important as water erosion for hillslopes subject to intensive agriculture (Van Oost et al., 2000). To demonstrate this, Table 8 shows that no tillage prior to cover crop planting represents a noticeable decrease in mean annual runoff, SY, and SL between 2021-2100 when compared to the winter wheat only scenario (Figures 10-12). In this respect, planting a cover crop with winter wheat represents the most sensible land management practice to balance future environmental and economic demands when no tillage is practised prior to cover crop planting.

4.3. Seasonal Changes in Soil Erosion

4.3.1. Climate Change Impacts

An earlier and longer muddy flooding season when compared to the baseline is consistently projected between 2021 and 2100 under current land management practices (Figure 8). The muddy flooding season begins around April and extends to November under each future time slice. Besides 2021-2040, the peak month of SY remains in August between 2041 and 2100. These results are consistent with Mullan et al. (2019) for an analogous catchment in Flanders under 1.5°C and 2°C warming using the mean of all model projections.

To quote from Mullan et al. (2016), “timing is everything”–- models that project highly for certain precipitation variables at a time that the soil surface is vulnerable will yield the highest SL and SY returns. The soil surface is typically most vulnerable between mid-April to August, marking the time it takes for summer crops to establish sufficient cover following planting. Consequently, Mullan et al. (2016) found that model projections of rainfall intensity (MX.5 P) correlated very strongly with projected SY such that this variable alone could confidently explain future SY projected by each model together with crop rotation dates. In contrast, the most dominant explanatory precipitation

684 variable in this study is the standard deviation of precipitation (SDEV P), which most closely explains
685 results in Figures 7 and 8. This is somewhat consistent with findings in Zhang (2012) where a larger
686 SDEV P typically provided more events with greater magnitudes of daily precipitation in WEPP, while
687 the opposite was true with a smaller SDEV P. The only exception is that Zhang (2012) also discussed
688 the impact of combining SDEV P with the skewness of precipitation (SKEW P). Figure 16 acts to
689 demonstrate that SDEV P alone can explain the SY results between 2021 and 2100, with R^2 values
690 ranging from 0.64 to 0.74 across all time intervals during the vulnerable months of May to August.
691 Rotating winter wheat with a summer crop the following year decreases this correlation. Winter
692 wheat provides sufficient cover during these typically 'vulnerable' months since planting occurs in
693 mid-October with harvesting in August. Appendix F details that R^2 values remain above 0.92 for each
694 of the time intervals when only summer crops are planted, given the consistently low soil surface
695 cover provided each year between April and August. Consequently, these results strongly suggest
696 that the variability in the probability of a wet day occurring within a given month largely determines
697 the SY response in WEPP.

698

699 #### 4.3.2. Alternative Land Use
700

701 The alternative land use scenarios offer differing months of soil surface vulnerability. Introducing
702 summer crops clearly extends the season of highest soil vulnerability. While seasonal changes in SY
703 remain similar to projections under current land management practices, subtle differences under
704 summer crops only are explained by the absence of winter wheat (Figure 15). Higher SY in October
705 and November when compared to existing land use between 2021 and 2100 is granted by harvesting
706 of the summer crops in October. The soil surface remains relatively bare and unprotected while the
707 cover crop establishes sufficient cover. It is likely that the spike in SY observed in June between 2021
708 and 2040 is also explained by the poor soil cover provided by the summer crops when compared to
709 winter wheat rotations during this month (Figure 15).

710 Alternatively, the shortened seasons of increased SY demonstrated for the winter wheat only and
711 winter wheat with cover crop scenarios indicate high susceptibility to tillage operations. High SY in
712 November between 2021 and 2100 for the winter wheat only scenario corresponds to tillage
713 practices in November (Figure 13), while the additional tillage practice required for the winter wheat
714 with cover crop scenario in September corresponds to the rise in SY for this month between 2021
715 and 2100 (Figure 14). As seen for mean annual changes (Table 8), Figure 17 shows that no tillage
716 prior to cover crop planting with winter wheat drastically reduces SY between 2021-2100. While

seasonal SY is barely apparent when plotted with existing land management under the same climatic conditions, peaks in SY coincide with tillage practices prior to winter wheat planting in November. It is impractical to correlate SDEV P with SY for each of these land use scenarios given that the longest season of high SY projected between 2021 and 2100 does not exceed three months.

4.4. Implications for Future Mitigation Planning

Existing mitigation measures in place at the Heulen Gracht to manage soil erosion and muddy flooding have remained effective under current climatic conditions. Previous research found that considerable re-infiltration caused runoff coefficients to decrease by a mean of 60%, while sediment discharge also decreased by 93% between the inflow and outflow of the grassed waterway (Evrard, 2008). These mitigation measures were cost-effective within three years, despite being designed for a 20 year period (Evrard et al., 2007a, 2008). While this 20-year period is reaching an end, results in this study reveal that existing mitigation measures may remain resilient to climatic conditions during 2021-2040 under current land management practices. Regular monitoring and maintenance of these mitigation measures may remain sufficient between 2021 and 2040.

However, it is very clear that climatic conditions during 2041-2100 will pose a considerable threat to the resilience of these existing mitigation measures, which is consistent with previous research for a separate Belgian catchment (Mullan et al., 2019). This study finds that a range of alternative land management practices will be highly effective between 2041 and 2100, such that soil erosion rates and runoff generation between 2041 and 2100 under each of these alternative land use scenarios will represent an improvement from observed measurements under current climatic conditions and land use. However, despite high efficacy, changes to existing farming practices may represent a more radical solution when compared to adapting current mitigation measures and perhaps introducing additional measures. Mullan et al. (2016) previously suggested minor modifications to the dimensions of currently installed mitigation measures as an effective approach under future climatic conditions.

The most viable mitigation strategy will largely be determined by farmer cooperation. It is important to provide a wide range of feasible solutions so that the interests of all relevant decision makers can be easily satisfied. This study reveals that only planting winter wheat represents a highly effective economical and environmentally sensitive additional option to curative mitigation measures for reducing off-site damages from soil erosion and muddy flooding under a changing climate.

4.5. Limitations

WEPP is widely applied within climate change-soil erosion research, with success demonstrated in a range of studies (e.g. Mullan et al., 2016; Stolpe, 2005). However, there are several notable limitations associated with hillslope scale analysis.

The first difficulty is concerned with the need for hillslope specific measurements of SY, SL and runoff over several years for adequate model validation. Instead, soil erosion is typically measured at the outlet of the catchment for heavily impacted study areas. While this is certainly the case for the Heulen Gracht, Mullan et al. (2019) also discussed the absence of measured hillslope specific data for another analogous catchment in Flanders where it was necessary to make volumetric calculations made on sedimentation zones following a single muddy flooding event to validate WEPP results. This validation is also limited to mean annual SY at the catchment outlet cited in Evrard (2008), while long-term information for SL and runoff is difficult to come by. The absence of hillslope-specific measurements of runoff coefficients certainly limits analysis. For instance, a previous study (Evrard, 2008) revealed that grassland compaction differs across the Heulen Gracht. Grass buffer strips and grassed waterways often act as transport routes for heavy machinery, such that these areas typically generate higher runoff coefficients than cultivated land due to increased compaction. It is important that regular monitoring and data collection at these selected hillslopes are undertaken to develop detailed databases to assist future modelling development, so that hillslope specific information – such as runoff coefficients – are adequately represented. Otherwise, model validation described in Section 3.1 represents a strong attempt to validate modelled hillslope diagnostics, given the absence of longer-term site-specific hillslope data. Similarly, collection of additional field data to carefully estimate baseline effective hydraulic conductivity is needed so that WEPP can suitably simulate the long-term effects of soil macropores forming, which may impact infiltration rates and runoff over time.

Lastly, hillslope scale analysis fails to consider the hydrological connectivity of the landscape, which is commonly recognised as a significant contributor to the scale of soil erosion and muddy flooding (e.g. Boardman and Vandaele, 2016; Boardman et al., 2019). While WEPP validation was completed using watershed mode, simulations only included two hillslopes because of field access limitations. Extensive mitigation at the GBS Hillslope made it difficult to clearly analyse the impact of future climatic changes on soil erosion, such that only the less-mitigated the GWW Hillslope was chosen for detailed analysis (Figures 6-16). Hillslope scale analysis is unable to provide spatial patterns of

782 sediment yield and the relative contribution of sediment from rills, gullies, and interill areas (Mullan
783 et al., 2019). Analysis completed at a catchment scale is valuable to identify hotpots for soil erosion
784 that could benefit from mitigation adaptation or instalment.

785

786 5. Conclusions

787

788 Findings in this study represent an advance from previous research examining soil erosion by water.
789 This study presents the first targeted methodology (the PPE method) to efficiently select suitable
790 climate models for simulating soil erosion by water. A sensible range of likely scenarios is generated,
791 since PPE blends and precisely transforms both envelope-based and past-performance approaches.
792 The highest range in future (2081-2100) mean annual SY, SL and runoff was projected by PPE, when
793 compared to other popular model selection methods. Relevant impact sectors such as soil erosion
794 and muddy flooding, and other hydrological phenomena, should consider applying this method to
795 assess the impact of future climatic changes.

796 This study also examined the role of future land use changes under a changing climate, which is
797 commonly neglected in recent soil erosion modelling research and has never been assessed for
798 muddy flooding specifically. This study finds that the magnitude of erosion events will increase
799 between 2021-2100 with considerable increases from 2041 under existing land use, while a longer
800 muddy flooding season is projected. The frequency of high magnitude events will also increase for
801 each return period up to a 1 in 100-year event under both the mean and maximum of all modelled
802 projections. A decrease in mean sediment yield and daily precipitation from the baseline is only
803 shown for a 1 in 100-year event under 2021-2040 climatic conditions. Current mitigation measures
804 may remain effective between 2021 and 2040 but will certainly require substantial adaptation to
805 continue to control soil erosion and muddy flooding under 2041-2100 climatic conditions. This is
806 unless commonly planted summer crops are replaced by winter wheat, which represents an
807 economical and environmentally viable alternative. Winter wheat induces considerable reductions in
808 SY, SL and runoff while providing a much shorter season of high SY. Efforts to adapt and introduce
809 mitigation measures – such as grass buffer strips, grassed waterways, detention ponds, and earth
810 dams – remain a sensible strategy to combat future soil erosion but winter wheat should also be
811 considered alongside these options, especially under the circumstance that summer crops will
812 become increasingly less profitable.

Overall, this research illuminates the importance of carefully tuned climate model selection and land use changes for modelling future soil erosion by water so the best- and worst-case scenarios can be adequately prepared for under a changing climate.

Acknowledgements

The authors would like to thank the Department for the Economy (DfE), who provided the lead author with a PhD scholarship to complete this research.

References

Alduchov, O. A., & Eskridge, R. E. (1996). Improved Magnus form approximation of saturation vapor pressure. *Journal of Applied Meteorology, (35)4*, 601–609. https://doi.org/10.1175/1520-0450(1996)035%3C0601:IMFAOS%3E2.0.CO;2

Arnell, N. W., Hudson, D. A., & Jones, R. G. (2003). Climate change scenarios from a regional climate model: Estimating change in runoff in southern Africa. *Journal of Geophysical Research D: Atmospheres, 108*(D16), 4519. https://doi.org/10.1029/2002jd002782

Ascough, J. C. II, Baffaut, C., Nearing, M. A., & Flanagan, D. C. (1995). Watershed model channel hydrology and erosion processes. Chapter 13 in (Flanagan, D. C. & Nearing, M. A., eds.): USDA Water Erosion Prediction Project (WEPP) Hillslope Profile and Watershed Model Documentation. NSERL Report No. 10, National Soil Erosion Research Laboratory, USDA Agricultural Research Service, West Lafayette, Indiana. pp. 13.1-13.20. https://www.ars.usda.gov/ARSUserFiles/50201000/WEPP/chap13.pdf

Bakker, M. M., Govers, G., & Rounsevell, M. D. A. (2004). The crop productivity-erosion relationship: An analysis based on experimental work. *Catena*, *57(1)*, 55–76. https://doi.org/10.1016/j.catena.2003.07.002

Beckers, V., Beckers, J., Vanmaercke, M., Van Hecke, E., Van Rompaey, A., & Dendoncker, N. (2018). Modelling farm growth and its impact on agricultural land use: A country scale application of an agent-based model. *Land, 7(3)*, 109, 19 pp. https://doi.org/10.3390/land7030109

Bielders, C. L., Ramelot, C., & Persoons, E. (2003). Farmer perception of runoff and erosion and extent of flooding in the silt-loam belt of the Belgian Walloon Region. *Environmental Science & Policy, 6(1)*, 85–93. https://doi.org/10.1016/S1462-9011(02)00117-X

Biemans, H., Speelman, L. H., Ludwig, F., Moors, E. J., Wiltshire, A. J., Kumar, P., Gerten, D., & Kabat, P. (2013). Future water resources for food production in five South Asian river basins and potential for adaptation - A modeling study. *Science of the Total Environment, 468–469*, S117– S131. https://doi.org/10.1016/j.scitotenv.2013.05.092

Boardman, J. (2021). How much is soil erosion costing us? *Geography, 106(1)*, 32–38. https://doi.org/10.1080/00167487.2020.1862584

Boardman, J., & Favis-Mortlock, D. (1993). Climate change and soil erosion in Britain. *The Geographical Journal, 159(2)*, 179–183. 852

Boardman, J., Ligneau, L., de Roo, A., & Vandaele, K. (1994). Flooding of property by runoff from agricultural land in northwestern Europe. *Geomorphology, 10(1–4)*, 183–196. https://doi.org/10.1016/0169-555X(94)90016-7

Boardman, J., & Vandaele, K. (2010). Soil erosion, muddy floods and the need for institutional memory. *Area, 42(4)*, 502–513. https://doi.org/10.1111/j.1475-4762.2010.00948.x

Boardman, J., & Vandaele, K. (2016). Effect of the spatial organization of land use on muddy flooding from cultivated catchments and recommendations for the adoption of control measures. *Earth Surface Processes and Landforms, 41(3)*, 336–343. https://doi.org/10.1002/esp.3793

Boardman, J., & Vandaele, K. (2020). Managing muddy floods: Balancing engineered and alternative approaches. *Journal of Flood Risk Management, 13(1)*, e12578. 10 pp. https://doi.org/10.1111/jfr3.12578

Boardman, J., Vandaele, K., Evans, R., & Foster, I. D. L. (2019). Off-site impacts of soil erosion and runoff: Why connectivity is more important than erosion rates. *Soil Use and Management, 35(2)*, 245–256. https://doi.org/10.1111/sum.12496

Bridges, E. M., & Oldeman, L. R. (1999). Global assessment of human-induced soil degradation. *Arid Soil Research and Rehabilitation, 13(4)*, 319–325. https://doi.org/10.1080/089030699263212

Butler, J. J. (2005). Muddy flooding on the South Downs. *Online Papers Archived by the Institute of Geography, School of Geosciences, University of Edinburgh.* http://www.era.lib.ed.ac.uk/handle/1842/830

Corbane, C., Andrieux, P., Voltz, M., Chadœuf, J., Albergel, J., Robbez-Masson, J. M., & Zante, P. (2008). Assessing the variability of soil surface characteristics in row-cropped fields: The case of Mediterranean vineyards in Southern France. *Catena, 72(1)*, 79–90. https://doi.org/10.1016/j.catena.2007.04.006

De Frutos Cachorro, J., Gobin, A., & Buysse, J. (2018). Farm-level adaptation to climate change: The case of the Loam region in Belgium. *Agricultural Systems, 165*, 164–176. https://doi.org/10.1016/j.agsy.2018.06.007

Evrard, O., Heitz, C., Liégeois, M., Boardman, J., Vandaele, K., Auzet, A. V., & Van Wesemael, B. (2010). A comparison of management approaches to control muddy floods in central Belgium, northern France and southern England. *Land Degradation and Development, 21(4)*, 322–335. https://doi.org/10.1002/ldr.1006 882

Evrard, O. (2008). *Muddy floods in the Belgian loess belt: Problems and solutions.*

Evrard, O., Bielders, C. L., Vandaele, K., & van Wesemael, B. (2007a). Spatial and temporal variation of muddy floods in central Belgium, off-site impacts and potential control measures. *Catena, 70(3)*, 443–454. https://doi.org/10.1016/j.catena.2006.11.011

Evrard, O., Persoons, E., Vandaele, K., & van Wesemael, B. (2007b). Effectiveness of erosion mitigation measures to prevent muddy floods: A case study in the Belgian loam belt. *Agriculture, Ecosystems and Environment, 118(1–4)*, 149–158. https://doi.org/10.1016/j.agee.2006.02.019 890

Evrard, O., Vandaele, K., van Wesemael, B., & Bielders, C. L. (2008). A grassed waterway and earthen dams to control muddy floods from a cultivated catchment of the Belgian loess belt. *Geomorphology, 100(3–4)*, 419–428. https://doi.org/10.1016/j.geomorph.2008.01.010

Fazeli Farsani, I., Farzaneh, M. R., Besalatpour, A. A., Salehi, M. H., & Faramarzi, M. (2019). Assessment of the impact of climate change on spatiotemporal variability of blue and green water resources under CMIP3 and CMIP5 models in a highly mountainous watershed. *Theoretical and Applied Climatology, 136(1–2),* 169–184. https://doi.org/10.1007/s00704-018-2474-9

Finger, D., Heinrich, G., Gobiet, A., & Bauder, A. (2012). Projections of future water resources and their uncertainty in a glacierized catchment in the Swiss Alps and the subsequent effects on hydropower production during the 21st century. *Water Resources Research, 48*, W02521, 20 pp. https://doi.org/10.1029/2011WR010733

Flanagan, D.C., & Livingston, S.J. (1995). USDA-Water Erosion Prediction Project (WEPP) User Summary. NSERL Rep. No. 11, National Soil Erosion Research Laboratory, USDA Agricultural Research Service, West Lafayette, Indiana.

Flanagan, D. C., & Nearing, M. A. eds. (1995). USDA - Water Erosion Prediction Project (WEPP) Hillslope Profile and Watershed Model Documentation. NSERL Report No. 10, National Soil Erosion Research Laboratory, USDA-Agricultural Research Service, West Lafayette, Indiana. 298 pp. https://www.ars.usda.gov/midwest-area/west-lafayette-in/national-soil-erosion-research/docs/wepp/wepp-model-documentation/

Gobin, A. (2010). Modelling climate impacts on crop yields in Belgium. *Climate Research, 44(1)*, 55-68. https://doi.org/10.3354/cr00925

Gobin, A. (2012). Impact of heat and drought stress on arable crop production in Belgium. *Natural Hazards and Earth System Sciences, 12(6)*, 1911–1922. https://doi.org/10.5194/nhess-12-1911-2012

Gobin, A. (2018). Weather related risks in Belgian arable agriculture. *Agricultural Systems, 159*, 225-236. https://doi.org/10.1016/j.agsy.2017.06.009

Gosling, S. N., McGregor, G. R., & Lowe, J. A. (2009). Climate change and heat-related mortality in six cities Part 2: Climate model evaluation and projected impacts from changes in the mean and variability of temperature with climate change. *International Journal of Biometeorology, 53(1)*, 31-51. https://doi.org/10.1007/s00484-008-0189-9

Graves, A. R., Morris, J., Deeks, L. K., Rickson, R. J., Kibblewhite, M. G., Harris, J. A., Farewell, T. S., & Truckle, I. (2015). The total costs of soil degradation in England and Wales. *Ecological Economics, 119*, 399–413. https://doi.org/10.1016/j.ecolecon.2015.07.026

Hawkins, E., Osborne, T. M., Ho, C. K., & Challinor, A. J. (2013). Calibration and bias correction of climate projections for crop modelling: An idealised case study over Europe. *Agricultural and Forest Meteorology, 170*, 19–31. https://doi.org/10.1016/j.agrformet.2012.04.007

Haylock, M. R., Hofstra, N., Klein Tank, A. M. G., Klok, E. J., Jones, P. D., & New, M. (2008). A European daily high-resolution gridded data set of surface temperature and precipitation for 1950-2006. *Journal of Geophysical Research Atmospheres, 113*, D20119. https://doi.org/10.1029/2008JD010201

Heitz, C., Spaeter, S., Auzet, A. V., & Glatron, S. (2009). Local stakeholders' perception of muddy flood risk and implications for management approaches: A case study in Alsace (France). *Land Use Policy, 26(2)*, 443–451. https://doi.org/10.1016/j.landusepol.2008.05.008

IPCC. (2013). Climate Change 2013: The Physical Science Basis. Contribution of Working Group I to the Fifth Assessment Report of the Intergovernmental Panel on Climate Change. In T. F. Stocker, D. Qin, G. K. Plattner, M. Tignor, S. K. Allen, J. Boschung, A. Nauels, Y. Xia, V. Bex, & P. M. Midgley (Eds.), *Cambridge University Press, Cambridge, United Kingdom and New York, NY, USA.* https://doi.org/https://doi.org/10.1017/CBO9781107415324

Kattsov, V., Federation, R., Reason, C., Africa, S., Uk, A. A., Uk, T. A., Baehr, J., Uk, A. B., Catto, J., Canada, J. S., & Uk, A. S. (2013). Evaluation of climate models. *Climate Change 2013 the Physical Science Basis: Working Group I Contribution to the Fifth Assessment Report of the Intergovernmental Panel on Climate Change, 9781107057*, 741–866. https://doi.org/10.1017/CBO9781107415324.020

Knutti, R., Rugenstein, M. A. A., & Hegerl, G. C. (2017). Beyond equilibrium climate sensitivity. *Nature Geoscience,* 10, 727-736. https://doi.org/10.1038/NGEO3017

Kundzewicz, Z. W., Mata, L. J., Arnell, N. W., Döll, P., Jimenez, B., Oki, T., Şen, Z., & Shiklomanov, I. (2008). *The implications of projected climate change for freshwater resources and their management resources and their management. Hydrological Sciences Journal, 53(1), 3-10*. https://doi.org/10.1623/hysj.53.1.3

Laflen, J. M., Lane, L. J., & Foster, G. R. (1991). WEPP: A new generation of erosion prediction technology. *J. Soil Water Conserv., 46(1)*, 34-38. http://www.jswconline.org/content/46/1/34.short

Lenderink, G., & Van Meijgaard, E. (2008). Increase in hourly precipitation extremes beyond expectations from temperature changes. *Nature Geoscience, 1(8)*, 511–514. https://doi.org/10.1038/ngeo262

Li, P., Mu, X., Holden, J., Wu, Y., Irvine, B., Wang, F., Gao, P., Zhao, G., & Sun, W. (2017). Comparison of soil erosion models used to study the Chinese Loess Plateau. *Earth-Science Reviews, 170*, 17–30. https://doi.org/10.1016/j.earscirev.2017.05.005

Lutz, A. F., ter Maat, H. W., Biemans, H., Shrestha, A. B., Wester, P. & Immerzeel, W. W. (2016). Selecting representative climate models for climate change impact studies: an advanced envelope-based selection approach. *Int. J. Climatol., 36(12)*, 3988-4005. https://doi.org/10.1002/joc.4608

Maeda, E. E., Pellikka, P. K. E., Siljander, M., & Clark, B. J. F. (2010). Potential impacts of agricultural expansion and climate change on soil erosion in the Eastern Arc Mountains of Kenya. *Geomorphology, 123(3–4)*, 279–289. https://doi.org/10.1016/j.geomorph.2010.07.019

Minville, M., Brissette, F., Leconte, R. (2008). Uncertainty of the impact of climate change on the hydrology of a nordic watershed. *J. Hydrol., 358(1-2)*, 70-83. https://doi.org/10.1016/j.jhydrol.2008.05.033

Mullan, D. (2013). Soil erosion under the impacts of future climate change: Assessing the statistical significance of future changes and the potential on-site and off-site problems. *Catena, 109*, 234–246. https://doi.org/10.1016/j.catena.2013.03.007

Mullan, D., Favis-Mortlock, D., & Fealy, R. (2012). Addressing key limitations associated with modelling soil erosion under the impacts of future climate change. *Agricultural and Forest Meteorology, 156*, 18–30. https://doi.org/10.1016/j.agrformet.2011.12.004

Mullan, D., Matthews, T., Vandaele, K., Barr, I. D., Swindles, G. T., Meneely, J., Boardman, J., & Murphy, C. (2019). Climate impacts on soil erosion and muddy flooding at 1.5 versus 2°C warming. *Land Degradation and Development, 30(1)*, 94–108. https://doi.org/10.1002/ldr.3214

Mullan, D., Vandaele, K., Boardman, J., Meneely, J., & Crossley, L. H. (2016). Modelling the effectiveness of grass buffer strips in managing muddy floods under a changing climate. *Geomorphology, 270*, 102–120. https://doi.org/10.1016/j.geomorph.2016.07.012

Nearing, M. A., Deer-Ascough, L., & Laflen, J. M. (1990). Sensitivity analysis of the WEPP hillslope erosion model. *Transactions of the ASAE, 33(3)*, 839–849. https://doi.org/10.13031/2013.31409

Nearing, M. A., Jetten, V., Baffaut, C., Cerdan, O., Couturier, A., Hernandez, M., Le Bissonnais, Y., Nichols, M. H., Nunes, J. P., Renschler, C. S., Souchère, V., & Van Oost, K. (2005). Modeling response of soil erosion and runoff to changes in precipitation and cover. *Catena, 61(2–3)*, 131–154. https://doi.org/10.1016/j.catena.2005.03.007

Nicks, A. D., Lane, L. J., & Gander, G. A. (1995). Chapter 2. Weather Generator. In (Flanagan, D.C, & Nearing, M. A., eds.): USDA–Water Erosion Prediction Project (WEPP) Hillslope Profile and Watershed Model Documentation. NSERL Report No. 10, National Soil Erosion Research Laboratory, USDA-Agricultural Research Service, West Lafayette (pp. 2.1–2.22). https://www.ars.usda.gov/ARSUserFiles/50201000/WEPP/chap2.pdf 32

O'Neal, M. R., Nearing, M. A., Vining, R. C., Southworth, J., & Pfeifer, R. A. (2005). Climate change impacts on soil erosion in Midwest United States with changes in crop management. *Catena, 61*(2-3 SPEC. ISS.), 165–184. https://doi.org/10.1016/j.catena.2005.03.003

Panagos, P., Borrelli, P., Poesen, J., Ballabio, C., Lugato, E., Meusburger, K., Montanarella, L., & Alewell, C. (2015). The new assessment of soil loss by water erosion in Europe. *Environmental Science and Policy, 54*, 438–447. https://doi.org/10.1016/j.envsci.2015.08.012

Phai, D. D., Orange, D., Migraine, J., Toan, T. D., & Vinh, N. C. (2007). Applying GIS-assisted modelling to predict soil erosion for a small agricultural watershed within sloping lands in Northern Vietnam. In (Gebbie, L., Glendinning, A., Lefroy-Braun, R., & Victor, M. (Eds.)): Proceedings of the International Conference on Sustainable Sloping Lands and Watershed Management: Linking Research to Strengthen Upland Policies and Practices, National Agriculture and Forestry Research Institute of Lao PDR (NAFRI), Vientiane, Lao PDR. pp. 212-228.

Pierce, D. W., Barnett, T. P., Santer, B. D., & Gleckler, P. J. (2009). Selecting global climate models for regional climate change studies. *Proceedings of the National Academy of Sciences of the United States of America, 106(21)*, 8441–8446. https://doi.org/10.1073/pnas.0900094106

Pimentel, D. (2006). Soil erosion: A food and environmental threat. *Environment, Development and Sustainability, 8(1)*, 119–137. https://doi.org/10.1007/s10668-005-1262-8

Pimentel, D., Harvey, C., Resosudarmo, P., Sinclair, K., Kurz, D., McNair, M., Crist, S., Shpritz, L., Fitton, L., Saffouri, R., & Blair, R. (1995). Environmental and economic costs of soil erosion and conservation benefits. *Science, 267*(5201), 1117-1123. https://doi.org/10.1126/science.267.5201.1117

Risbey, J. S., & Entekhabi, D. (1996). Observed Sacramento Basin streamflow response to precipitation and temperature changes and its relevance to climate impact studies. *Journal of Hydrology, 184(3-4)*, 209–223. https://doi.org/10.1016/0022-1694(95)02984-2

Sardari, M. R. A., Bazrafshan, O., Panagopoulos, T., & Sardooi, E. R. (2019). Modeling the impact of climate change and land use change scenarios on soil erosion at the Minab Dam Watershed. *Sustainability, 11(12)*, 3353. https://doi.org/10.3390/su11123353

Scholz, G., Quinton, J. N., & Strauss, P. (2008). Soil erosion from sugar beet in Central Europe in response to climate change induced seasonal precipitation variations. *Catena, 72(1)*, 91–105. https://doi.org/10.1016/j.catena.2007.04.005

Sha, J., Li, X., & Wang, Z. L. (2019). Estimation of future climate change in cold weather areas with the LARS-WG model under CMIP5 scenarios. *Theoretical and Applied Climatology, 137(3–4)*, 3027–3039. https://doi.org/10.1007/s00704-019-02781-4

Stolpe, N. B. (2005). A comparison of the RUSLE, EPIC and WEPP erosion models as calibrated to climate and soil of south-central Chile. *Acta Agriculturae Scandinavica Section B: Soil and Plant Science, 55(1)*, 2–8. https://doi.org/10.1080/09064710510008568

Sun, Y., Solomon, S., Dai, A., & Portmann, R. W. (2007). How often will it rain? *Journal of Climate, 20(19)*, 4801–4818. https://doi.org/10.1175/JCLI4263.1

Taylor, K. E., Stouffer, R.J., & Meehl, G. A. (2012). An overview of CMIP5 and the experiment design. *Bulletin of the American Meteorological Society, 93 (4)* (November), 485–498. https://doi.org/10.1175/BAMS-D-11-00094.1

Valentin, C., Poesen, J., & Li, Y. (2005). Gully erosion: Impacts, factors and control. *Catena, 63(2–3)*, 132–153. https://doi.org/10.1016/j.catena.2005.06.001

Van Oost, K., Govers, G., & Desmet, P. (2000). Evaluating the effects of changes in landscape structure on soil erosion by water and tillage. *Landscape Ecology, 15(6)*, 577–589. https://doi.org/10.1023/A:1008198215674

Verstraeten, G., Poesen, J., Govers, G., Gillijns, K., Van Rompaey, A., & Van Oost, K. (2003). Integrating science, policy and farmers to reduce soil loss and sediment delivery in Flanders, Belgium. *Environmental Science and Policy, 6(1)*, 95–103. https://doi.org/10.1016/S1462-9011(02)00116-8

Yang, D., Kanae, S., Oki, T., Koike, T., & Musiake, K. (2003). Global potential soil erosion with reference to land use and climate changes. *Hydrological Processes, 17(14)*, 2913–2928. https://doi.org/10.1002/hyp.1441

Yu, B. (2003). An assessment of uncalibrated CLIGEN in Australia. *Agricultural and Forest Meteorology, 119(3–4)*, 131–148. https://doi.org/10.1016/S0168-1923(03)00141-2

Zhang, X. C. (2012). Verifying a temporal disaggregation method for generating daily precipitation of potentially non-stationary climate change for site-specific impact assessment. *International Journal of Climatology, 33(2)*, 326–342. https://doi.org/10.1002/joc.3425

Zhang, X. C. (2013). Adjusting skewness and maximum 0.5 hour intensity in CLIGEN to improve extreme event and sub-daily intensity generation for assessing climate change impacts. *Transactions of the ASABE, 56(5)*, 1703–1713. https://doi.org/10.13031/trans.56.10004

Zhang, X. C., Liu, W. Z., Li, Z., & Zheng, F. L. (2009). Simulating site-specific impacts of climate change on soil erosion and surface hydrology in southern Loess Plateau of China. *Catena, 79(3)*, 237–242. https://doi.org/10.1016/j.catena.2009.01.006

Zhang, X. C., & Nearing, M. A. (2005). Impact of climate change on soil erosion, runoff, and wheat productivity in central Oklahoma. *Catena, 61*(2-3 SPEC. ISS.), 185–195. https://doi.org/10.1016/j.catena.2005.03.009

Zhang, X. C., Nearing, M. A., Garbrecht, J. D., & Steiner, J. L. (2004). Downscaling monthly forecasts to simulate impacts of climate change on soil erosion and wheat production. *Soil Science Society of America Journal, 68(4)*, 1376–1385. https://doi.org/10.2136/sssaj2004.1376

Tables

Table 1: Hillslope characteristics necessary for model validation. Soil characteristics measured at depths of 0.6-1.8 m at the GBS Hillslope were kept constant for the GWW Hillslope simulations.

					Soil Sampling					
	Slope Length (m)	**Mean Slope Gradient (°)**	**Crop Rotation**	**Mitigation Measures**	**Depth (m)**	**No. Samples**	**Sand (%)**	**Silt (%)**	**Clay (%)**	**Organic (%)**
GBS Hillslope	65	8.1	Winter Wheat; Maize; Sugar Beet (44 m)	Grass Buffer Strip (21 m)	0.3	14	14.2	77	7.7	5.7
					0.6	1	10.8	79	10.3	4.4
					0.9	1	10.2	79	10.8	4.1
					1.2	1	10	80	10.1	3.7
					1.5	1	10.7	81	8.6	3.7
					1.8	1	10.3	81	8.7	3.2
GWW Hillslope	132.7	5	Winter Wheat; Maize; Sugar Beet (129.6 m)	Grassed Waterway (3.1 m)	0.3	11	14.3	78	7.7	4.5

Table 2: Description of CLIGEN input parameters and associated nomenclature (Mullan et al., 2019).

Parameter		Unit
Mean daily precipitation for each wet day for a given month	Mean P	in
Standard deviation of Mean P for a given month	SDev P	in
Skewness of Mean P for a given month	Skew P	ND[a]
Conditional probability of a wet day following a wet day for a given month	Pw/w	0-1
Conditional probability of a wet day following a dry day for a given month	Pw/d	0-1
Mean maximum temperature for a given month	AV TMAX	°F
Mean minimum temperature for a given month	AV TMIN	°F
Standard deviation of TMAX for a given month	SD TMAX	°F
Standard deviation of TMIN for a given month	SD TMIN	°F
Mean daily solar radiation for a given month	SOL.RAD	L/d[b]
Standard deviation of SOL.RAD for a given month	SD SOL	L/d[b]
Mean maximum daily 30-minute liquid precipitation intensity for a given month	MX.5P	In/hr
Mean daily dew point temperature for a given month	DEW PT	°F
Time to peak storm intensity	Time Pk	[c]
Mean percent of time that wind blows from 1 of 16 cardinal directions for a given month	% DIR [d]	%
Mean wind speed related to % DIR [c] for a given month	MEAN	m/s
Standard deviation of MEAN for a given month	SDev MEAN	m/s^{-1}
Skewness of MEAN for a given month	Skew MEAN	ND[a]
Mean percent of days that mean wind speed is less than 1 ms^{-1} for a given month	CALM	%

ND[a] – Nondimensional.

L/D[b] – Langleys/day.

[c] – Aside from Time Pk, all parameters represent the 12 calendar months shown along the columns.

[d] – Percent DIR refers to 16 different compass directions for wind direction. These are N, NNE, NE, ENE, E, ESE, SE, SSE, S, SSW, SW, WSW, W, WNW, NW, and NNW.

Table 3: Selected models for RCP4.5 and RCP8.5 following envelope-based selection. Models are ordered by distance to percentile, '1' representing least distance and '3' most distance. All models are r1i1p1 unless otherwise stated, where 'r' represents 'realization,' 'I' for 'initialisation' and 'p' for 'physics' within the CMIP5 project.

	RCP4.5			RCP8.5		
	1	2	3	1	2	3
Wet	GISS-E2-R r6i1p3	GISS-E2-R r6i1p1	MRI-CGCM3	IPSL-CM5A-LR r4i1p1	ACCESS1-3	IPSL-CM5A-LR r2i1p1
Dry	HADGEM2-AO	CNRM-CM5	HADGEM2-ES r2i1p1	CanESM2 r3i1p1	HADGEM2-ES r2i1p1	HADGEM2-ES

Table 4*:* Past performance analysis between observed and historical modelled data for models selected in Section 2.3.1. April to September is selected for analysis since these months are key months for muddy flooding. Listed models are coloured blue or red to represent RCP4.5 or RCP8.5, respectively. Values for the key precipitation characteristics are normalised, such that the highest value in each column equals 1. A rank of 1 equals closest performance to observed.

	Mean	SDev	Skew	P(w/w)	P(w/d)	NWD	Sum	Rank
MRI-CGCM3	0.37	0.01	0.26	0.57	0.53	0.59	2.33	1
IPSL-CM5A-LR r2i1p1	0.63	0.56	0.27	0.6	0.3	0.52	2.88	2
HADGEM2-ES r1i1p1	0.85	0.59	0.07	0.63	0.43	0.58	3.15	3
HADGEM2-ES r2i1p1	0.91	0.61	0.14	0.53	0.48	0.53	3.2	4
IPSL-CM5A-LR r4i1p1	0.98	1	0.22	0.43	0.25	0.4	3.28	5
ACCESS1-3	0.67	0	0.2	0.8	0.83	0.82	3.32	6
GISS-E2-R r6i1p3	0.45	0.18	0.38	1	0.95	0.99	3.95	7
GISS-E2-R r6i1p1	0.4	0.33	0.3	1	1	1	4.03	8
CNRM-CM5	0.61	0.4	1	0.8	0.75	0.8	4.36	9
CanESM2 r3i1p1	1	0.67	0.54	0.87	0.83	0.84	4.75	10

Table 5: Selected models from the PPE, ECS, and RG 1-3. Models are separated by RCP 4.5 and 8.5, selected randomly for RG 1-3. Otherwise, the order of the selected models within each RCP grouping displayed is random. Unless otherwise stated, all models are r1i1p1.

RCP4.5	RCP8.5
PPE	
MRI-CGCM3	IPSL-CM5A-LR r2i1p1
HADGEM2-ES r2i1p1	HADGEM2-ES r1i1p1
GISS-E2-R r6i1p3	IPSL-CM5A-LR r4i1p1
ECS	
GFDL-ESM2G	GFDL-CM3
GFDL-ESM2M	ACCESS1-0
GISS-E2-H	CSIRO-Mk3-6-0
RG1	
GISS-E2-R r6i1p3	IPSL-CM5A-LR r4i1p1
HADGEM2-ES r2i1p1	HADGEM2-ES r1i1p1
IPSL-CM5B-LR	CanESM2 r3i1p1
RG2	
MRI-CGCM3	ACCESS1-0
GFDL-ESM2M	GFDL-CM3
IPSL-CM5A-MR	CNRM-CM5
RG3	
GISS-E2-H	MIROC5
IPSL-CM5A-MR	IPSL-CM5A-LR r2i1p1
GFDL-ESM2G	CSIRO-Mk3-6-0

Table 6: Details of modifications required for key CLIGEN parameters to represent future climate changes.

CLIGEN Parameter	Derivation Method
Mean P	Equations 3 and 4
SDev P	Calculated from future Mean P
SKEW P	Calculated from future Q99
P(W/W)	See Section 2.5.
P(W/D)	See Section 2.5.
AV TMAX	Modified from future AV TMAX
AV TMIN	Modified from future AV TMIN
TMAX SD	Calculated from future AV TMAX
TMIN SD	Calculated from future AV TMIN
SOL.RAD	Linear regression – plotted against future AV TMAX
SD.SOL	Linear regression – plotted against future AV TMAX
MX.5P	Linear regression – plotted against future AV TMIN
DEW PT	Linear regression – plotted against future AV TMIN
Time PK	Linear regression – plotted against future SDev P

Table 7: Comparing the range (highest minus lowest model value) in sediment yield (SY) and daily precipitation (Pr.) projected by each model selection method at Hillslopes 1 and 2 for different return period intervals. The highest projected range for each return period interval has been coloured red.

		Range	
	Return Period	**SY (t/ha)**	**Precipitation (mm)**
PPE	2	4.1	18.3
	5	11.8	27.3
	10	16.3	35
	20	25.4	45.6
	25	27	53.8
	50	35.7	64.4
	100	52.1	85.1
ECS	2	0.9	6.3
	5	4.2	9.3
	10	7.9	13.4
	20	10	16.3
	25	14.7	20.3
	50	21.2	24.4
	100	44.1	30.5
RG1	2	3.7	10.3
	5	8.8	16.8
	10	11.6	20.1
	20	19.3	29.6
	25	20.4	33.4
	50	29.2	31.6
	100	42.5	38.9
RG2	2	2.7	20.4
	5	8.4	28.9
	10	15.2	37.2
	20	23.3	48.6
	25	23	57.6
	50	30.9	75.5
	100	29.9	89.8
RG3	2	0.2	9.6
	5	3.3	13.3
	10	5.9	18.5
	20	9.5	23.6
	25	10.4	28.4
	50	21.8	34.7
	100	49.2	44.9

Table 8: Mean annual sediment yield (SY), soil loss (SL) and runoff between 2021 and 2100 for the winter wheat with cover crop scenario when no tillage prior to cover crop planting is practised. 'Change' represents the relative difference from the winter wheat only scenario under the same climatic conditions.

	Runoff (mm)	Change (mm)	Soil loss (kg/m^2)	Change (kg/m^2)	Sediment Yield (t/ha)	Change (t/ha)
2021-2040	1.72	-0.08	0.00	-0.06	0.01	-0.19
2041-2060	3.35	-0.55	0.02	-0.15	0.08	-0.48
2061-2080	3.39	-0.29	0.04	-0.16	0.11	-0.65
2081-2100	1.72	-6.28	0.00	-0.37	0.01	-0.95

Figures

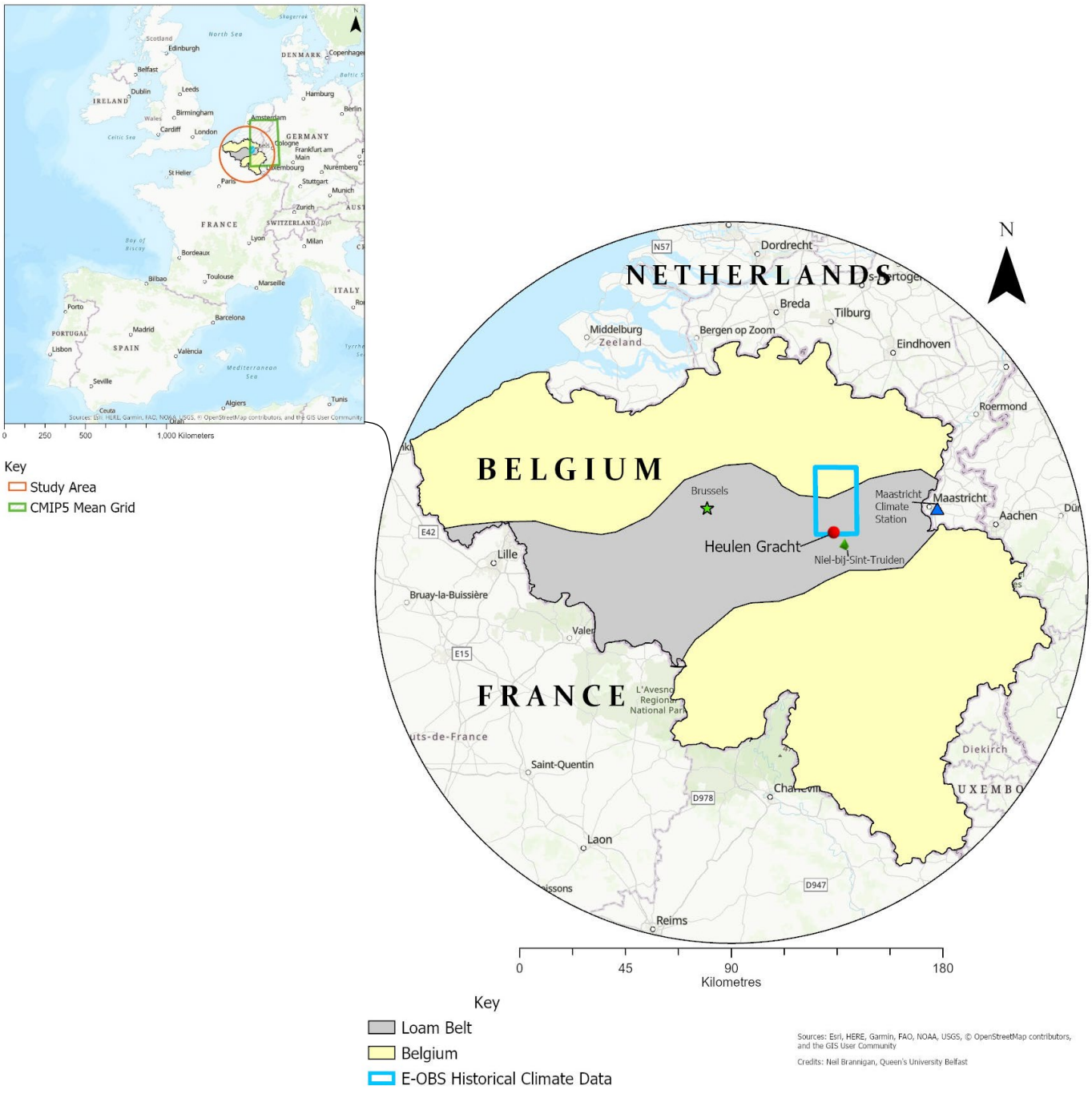

Figure 1: The location of the study area within the Belgian loess belt. Relevant climate information is also indicated.

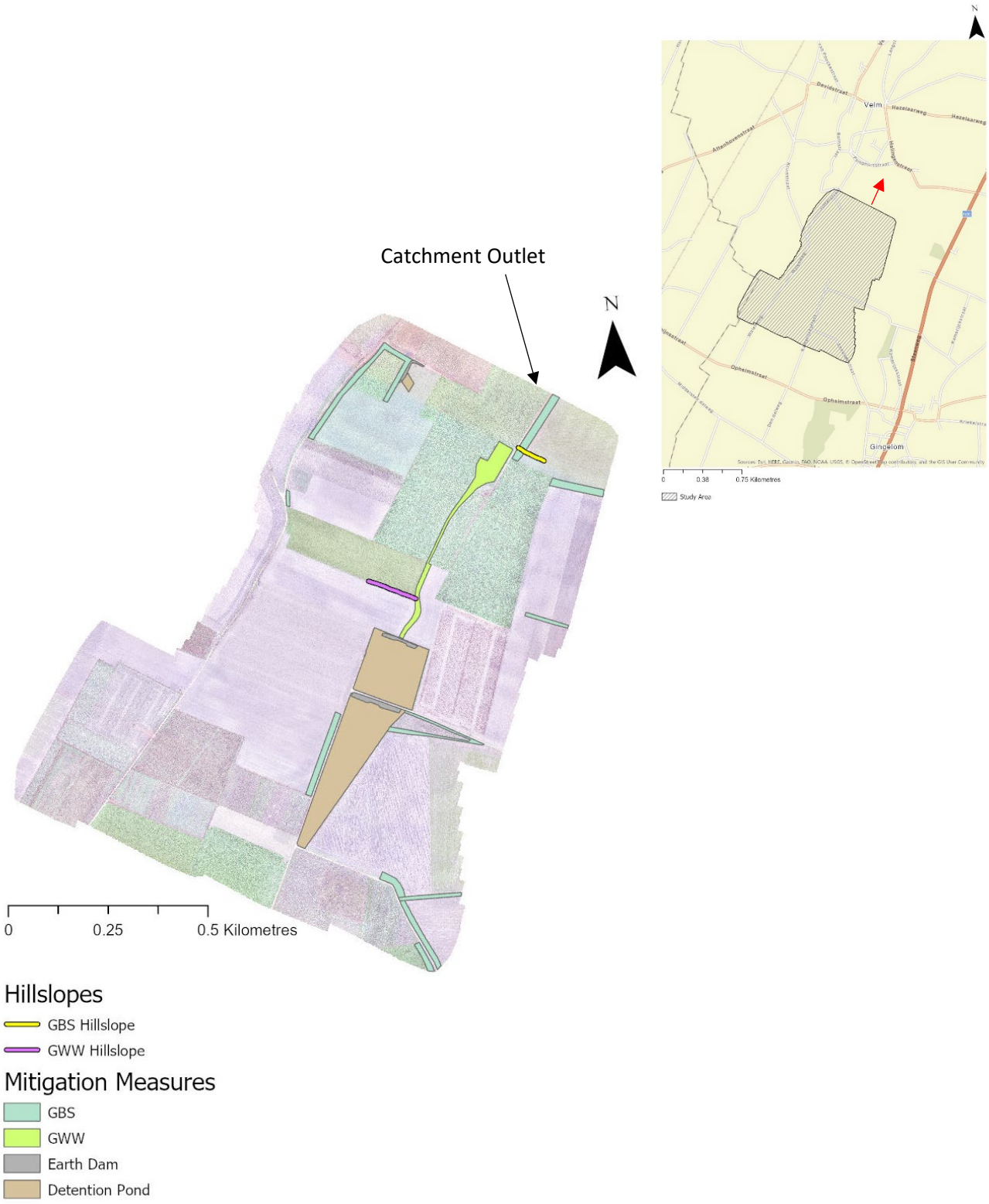

Figure 2: Location of existing mitigation measures across the study area, along with key hillslopes. The catchment outlet drains towards Velm Village, as indicated by the red arrow displayed on the street map insert.

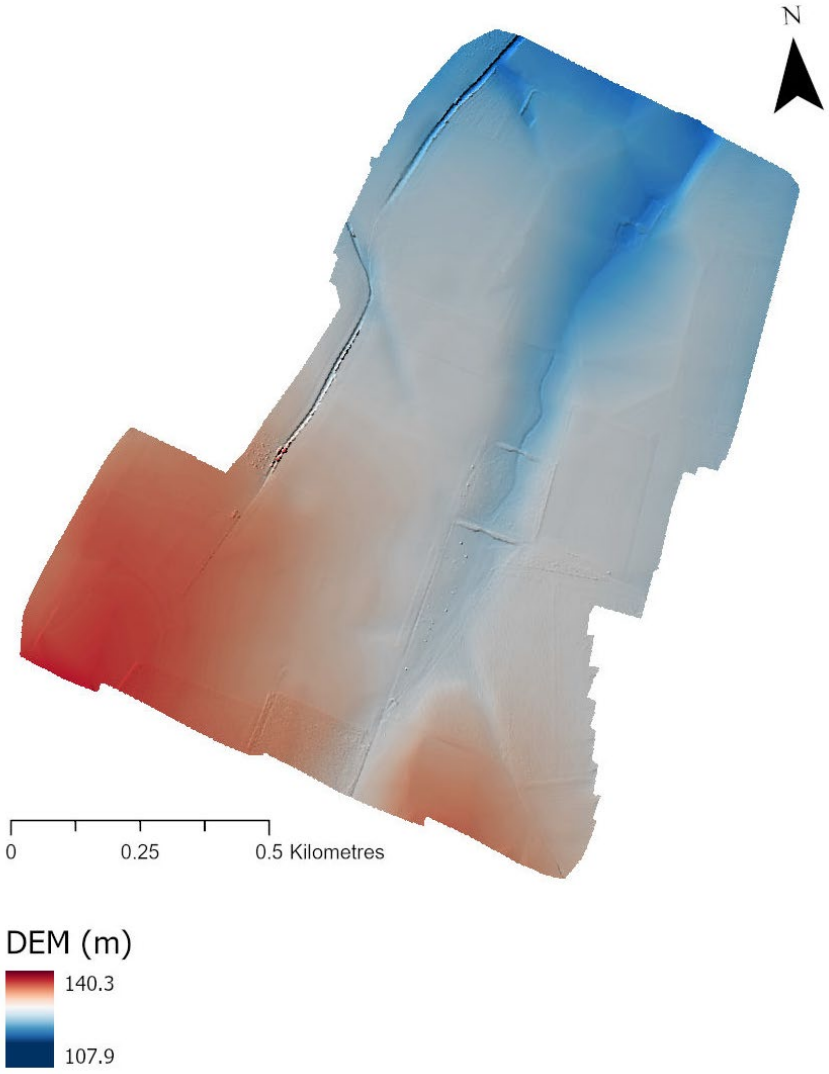

Figure 3*:* Digital elevation model (DEM) of the study area. The catchment thalweg is clearly delimited by the lowest elevation values.

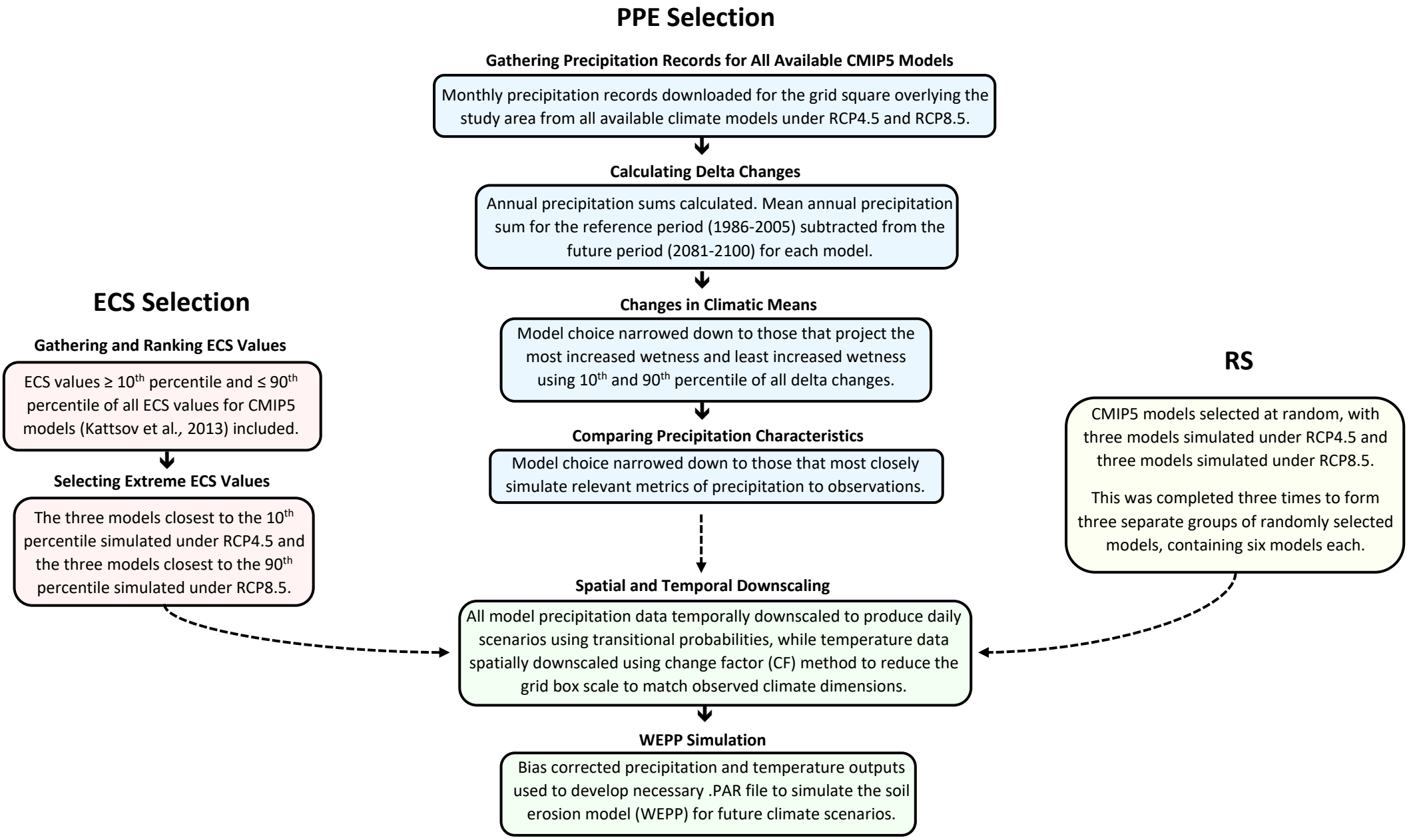

Figure 4: Summary of steps provided for all climate model selection methods to project climatic conditions for the future period (2081-2100) and simulate in a soil erosion model.

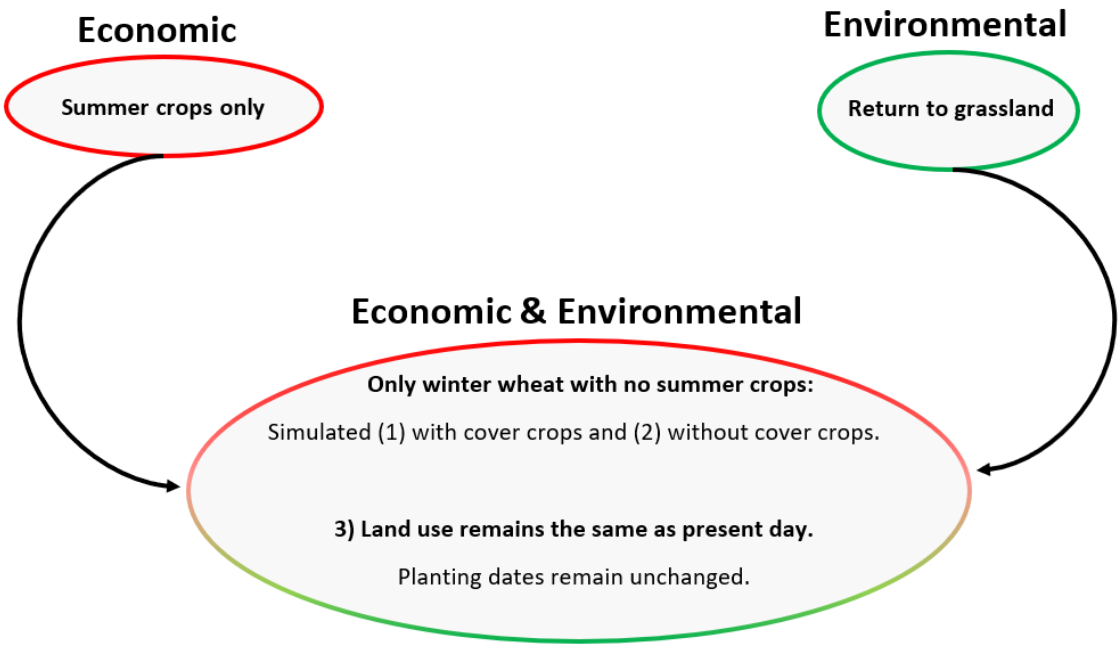

Figure 5: Conceptual model outlining the various land management scenarios applied in this study. These scenarios are divided into economic, environmental, and several economic-environmental scenarios.

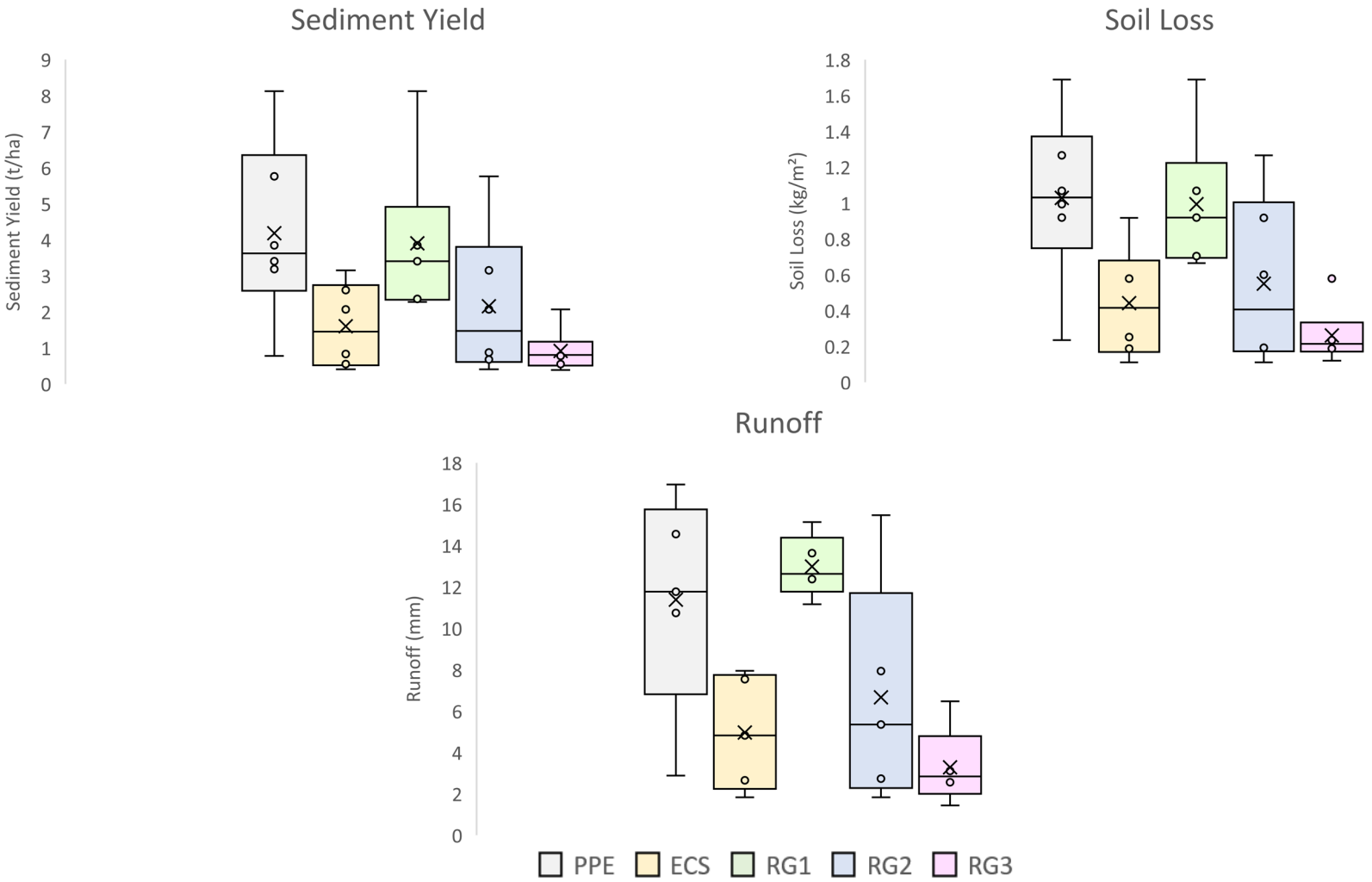

Figure 6: Projected ranges in sediment yield, soil loss, and runoff provided by each climate model selection method between 2081-2100 for the GWW Hillslope. The median value is represented by the horizontal line inside the box; 'x' marks the mean value; the circular dots represent Q1 (lower dot) and Q3 (upper dot); and the maximum and minimum values are denoted by the top and bottom whiskers, respectively.

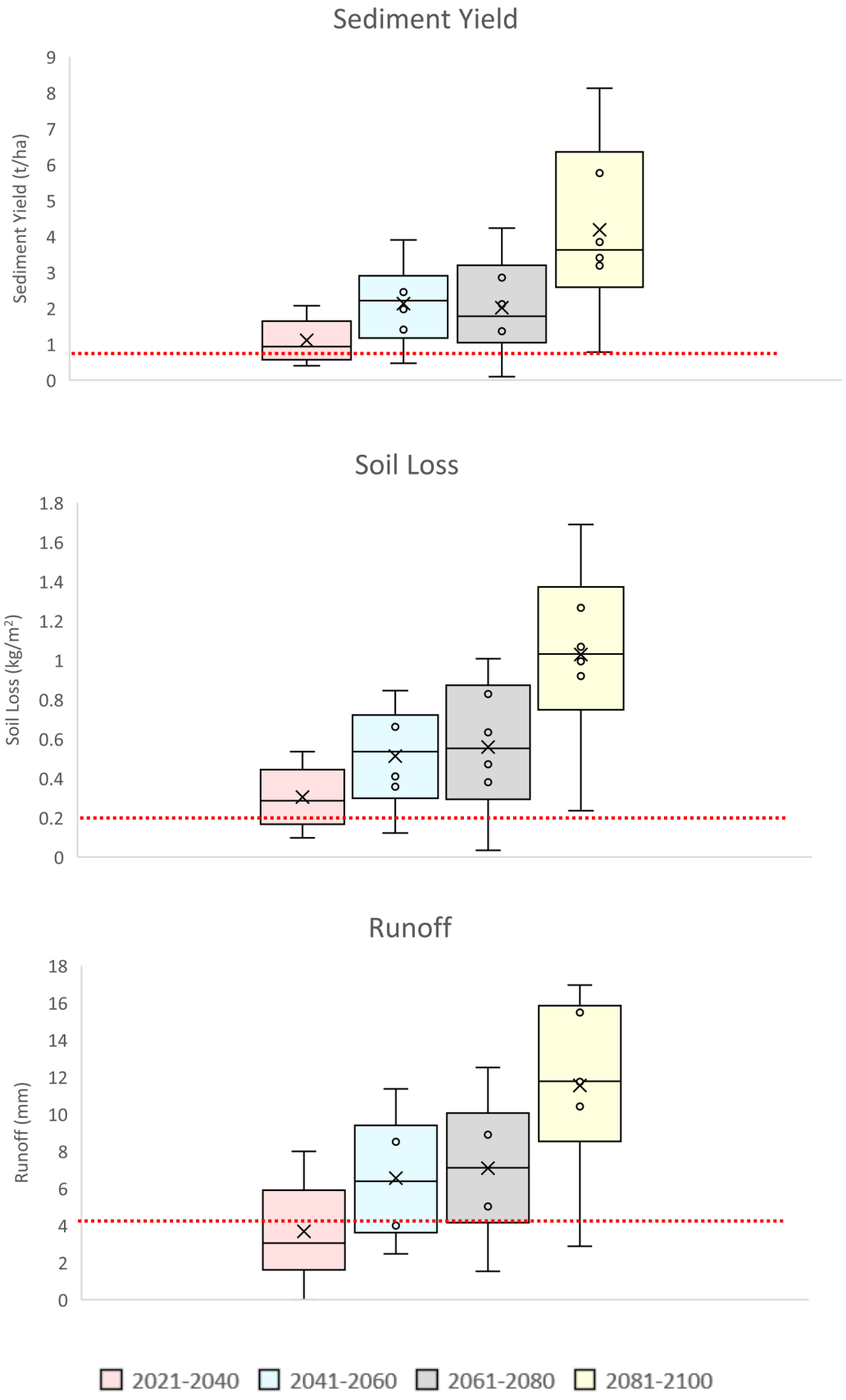

Figure 7: Mean annual changes in sediment yield (SY), soil loss (SL) and runoff between 2021 and 2100 for the GWW Hillslope. Baseline measurements for each of these respective diagnostics are represented by the red dotted line.

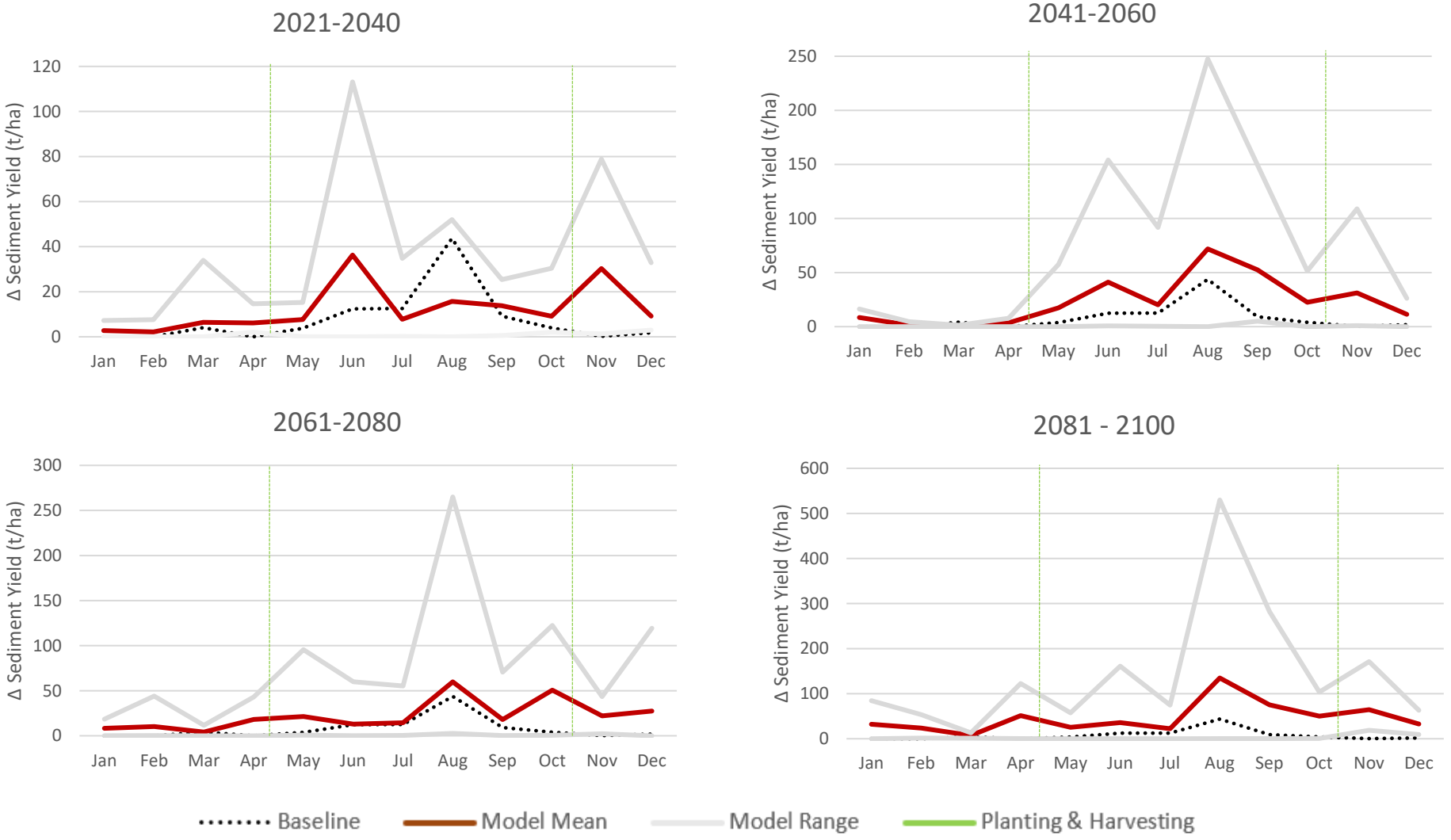

Figure 8: Seasonal changes in mean modelled sediment yield (SY) in kg/m from the baseline (E-OBS) between 2021-2100 for the GWW Hillslope. The model range is also displayed for each month, while planting and harvesting dates are also indicated.

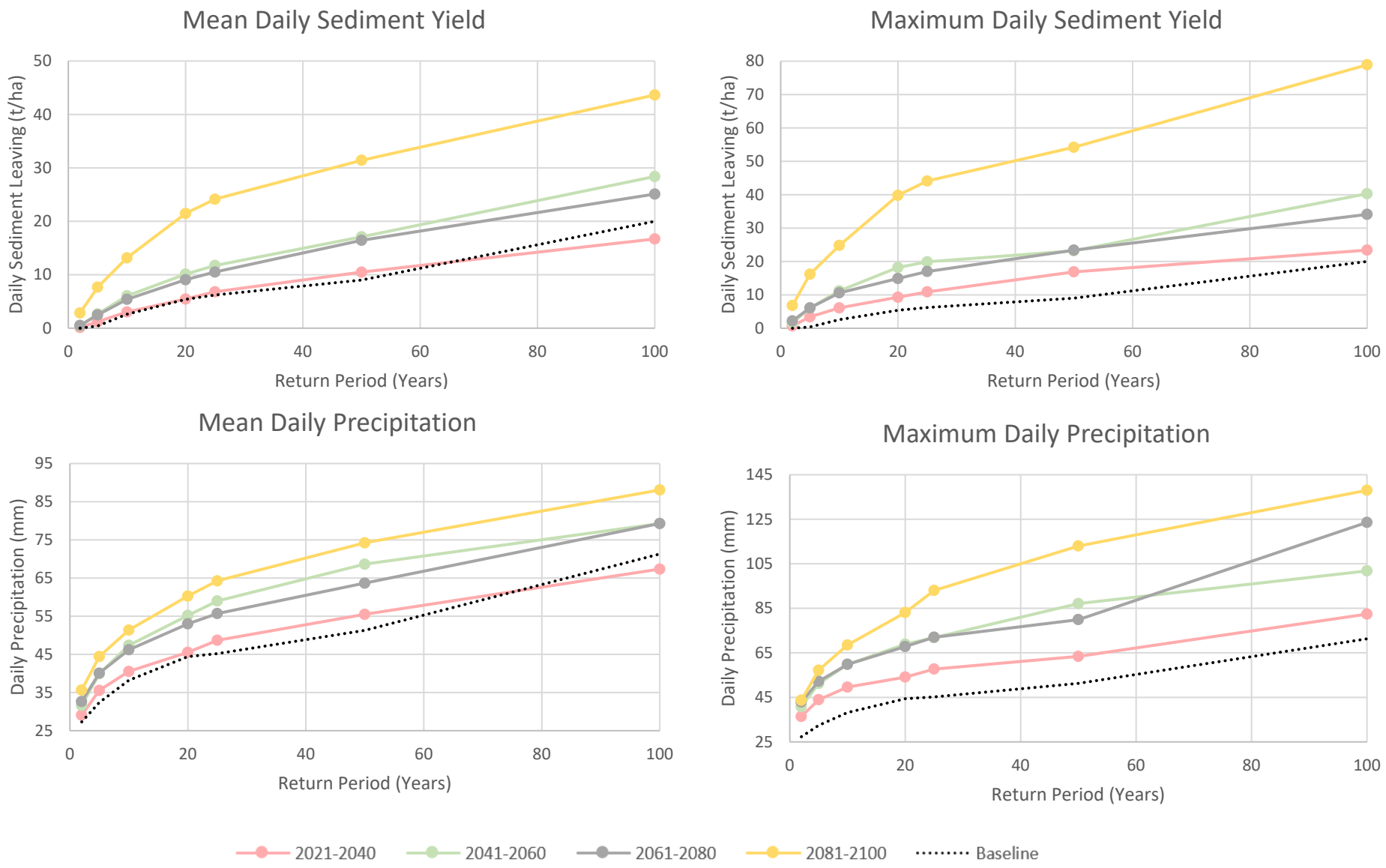

Figure 9: Mean and maximum modelled return periods for sediment yield (SY) and daily precipitation for the GWW Hillslope.

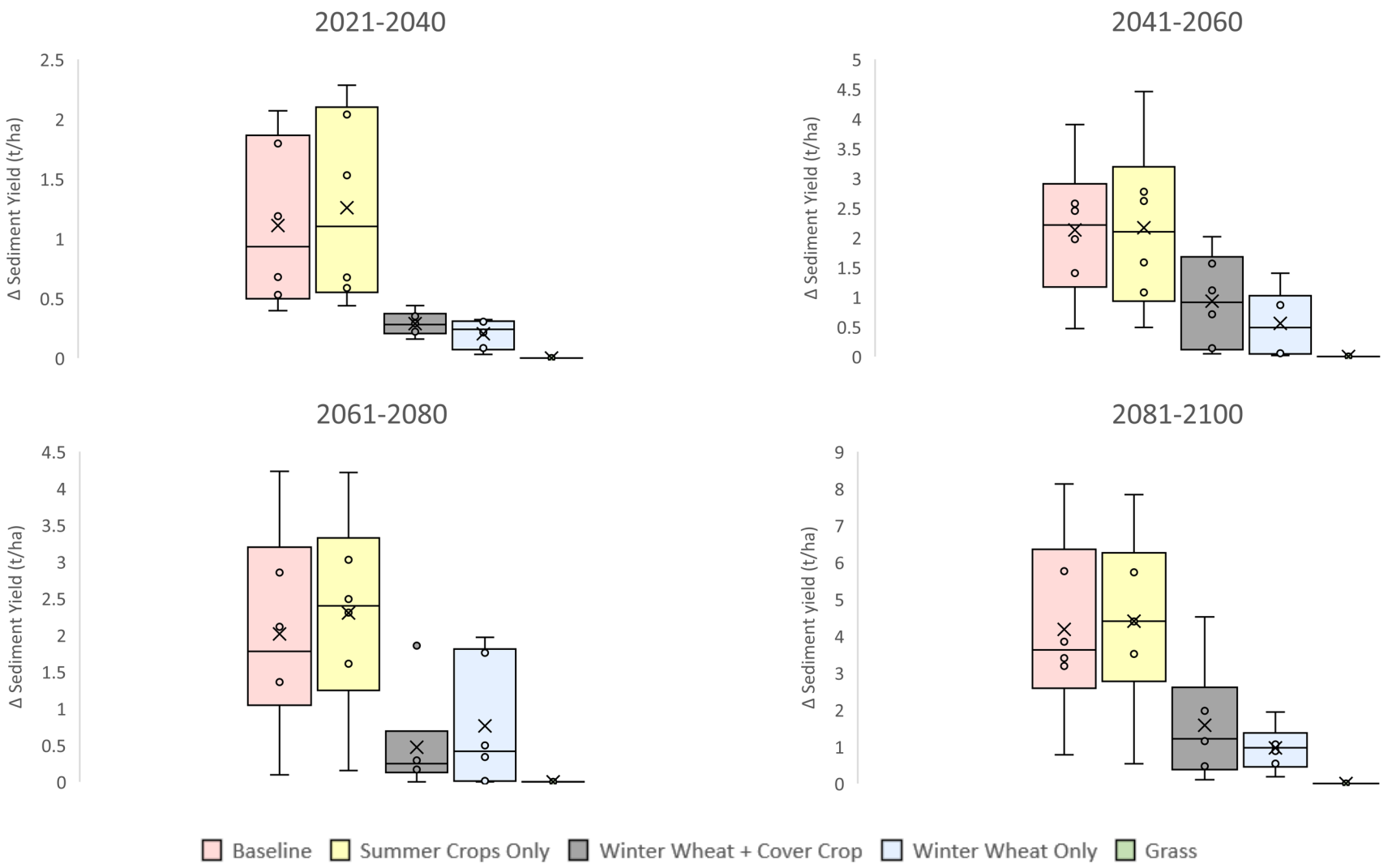

Figure 10: Mean annual changes in sediment yield between 2021 and 2100, demonstrated for each land use scenario.

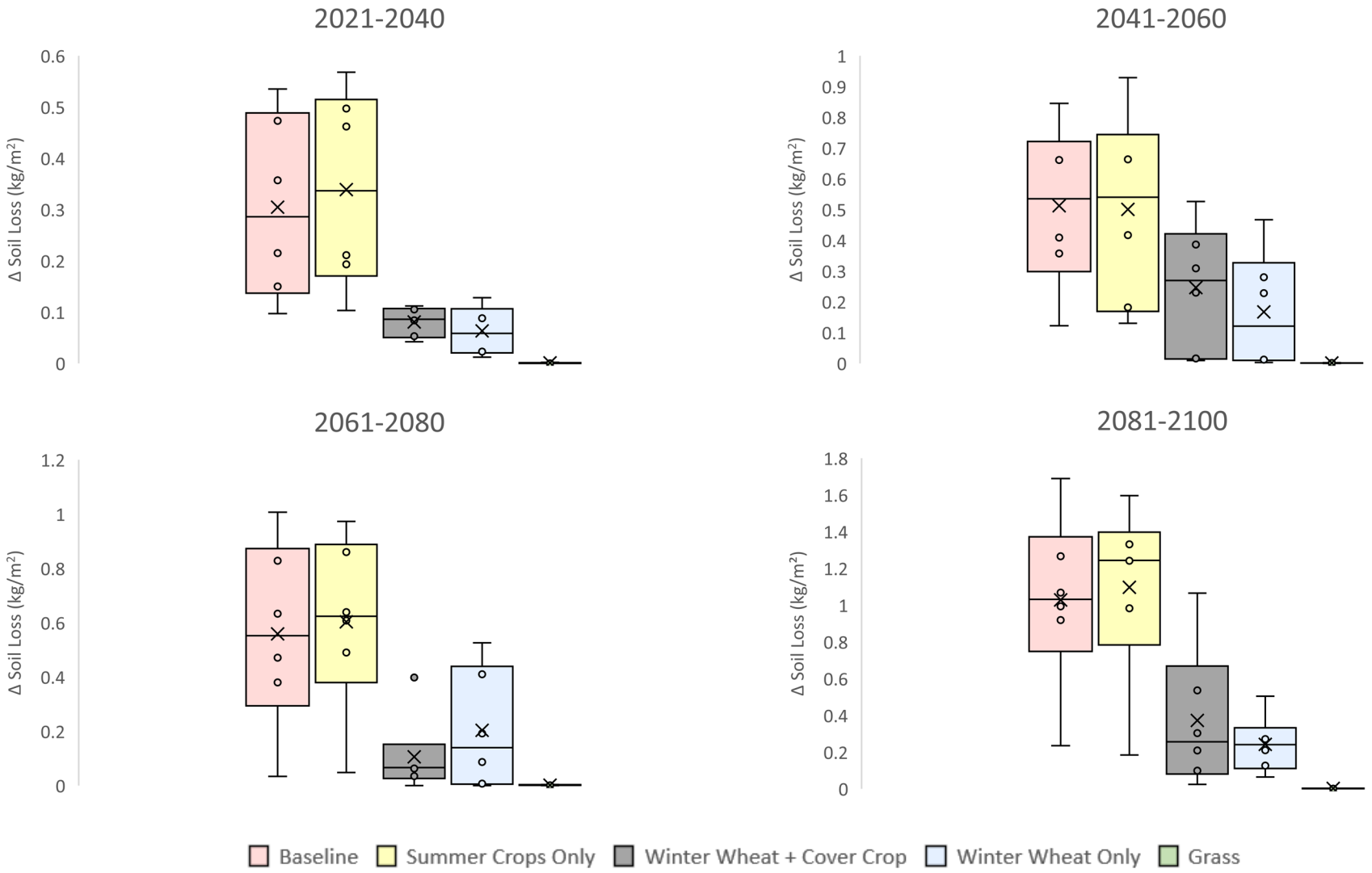

Figure 11: Same as for Figure 10, except for soil loss (SL) for the GWW Hillslope.

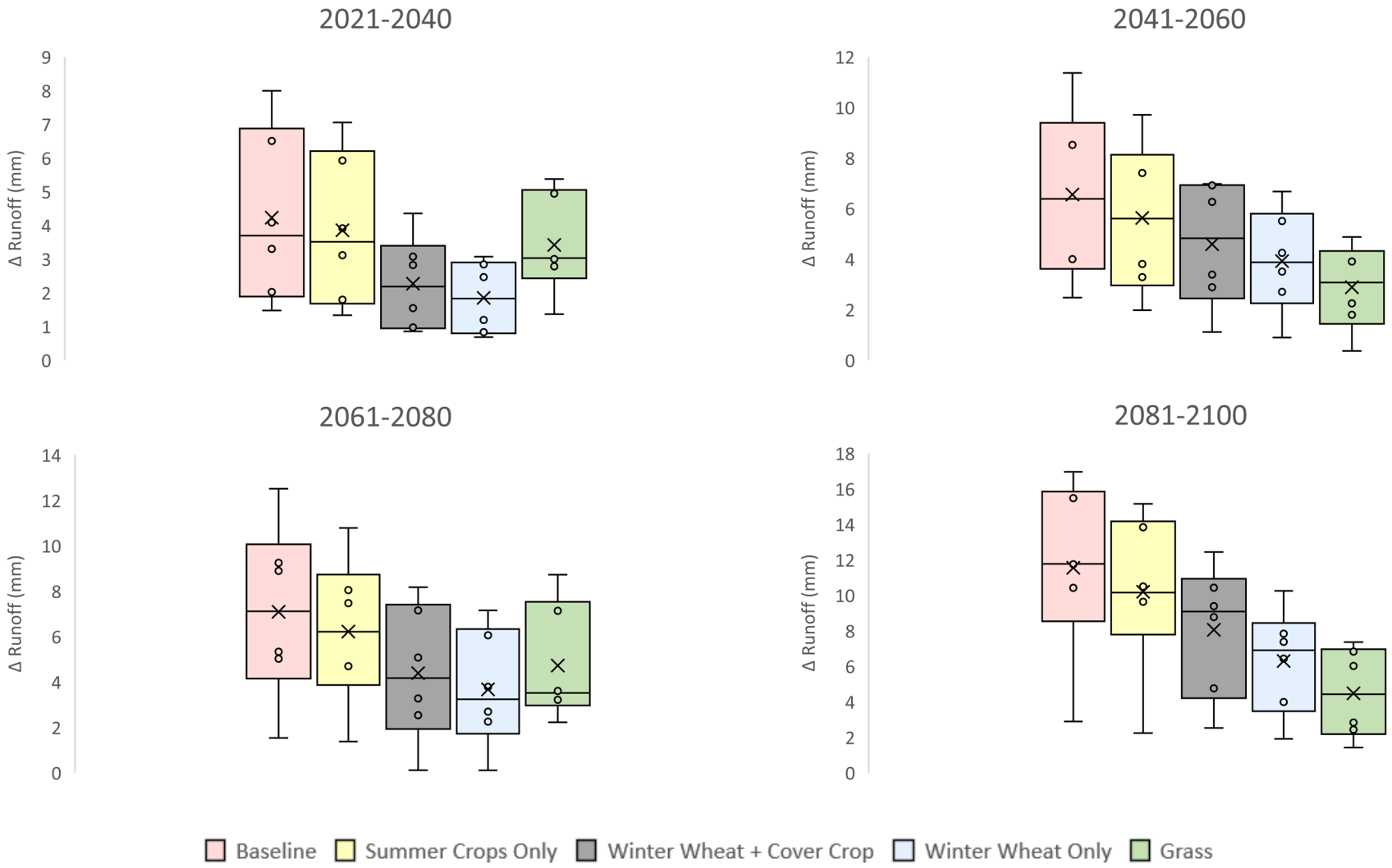

Figure 12: Same as for Figure 10, except for runoff (mm) for the GWW Hillslope.

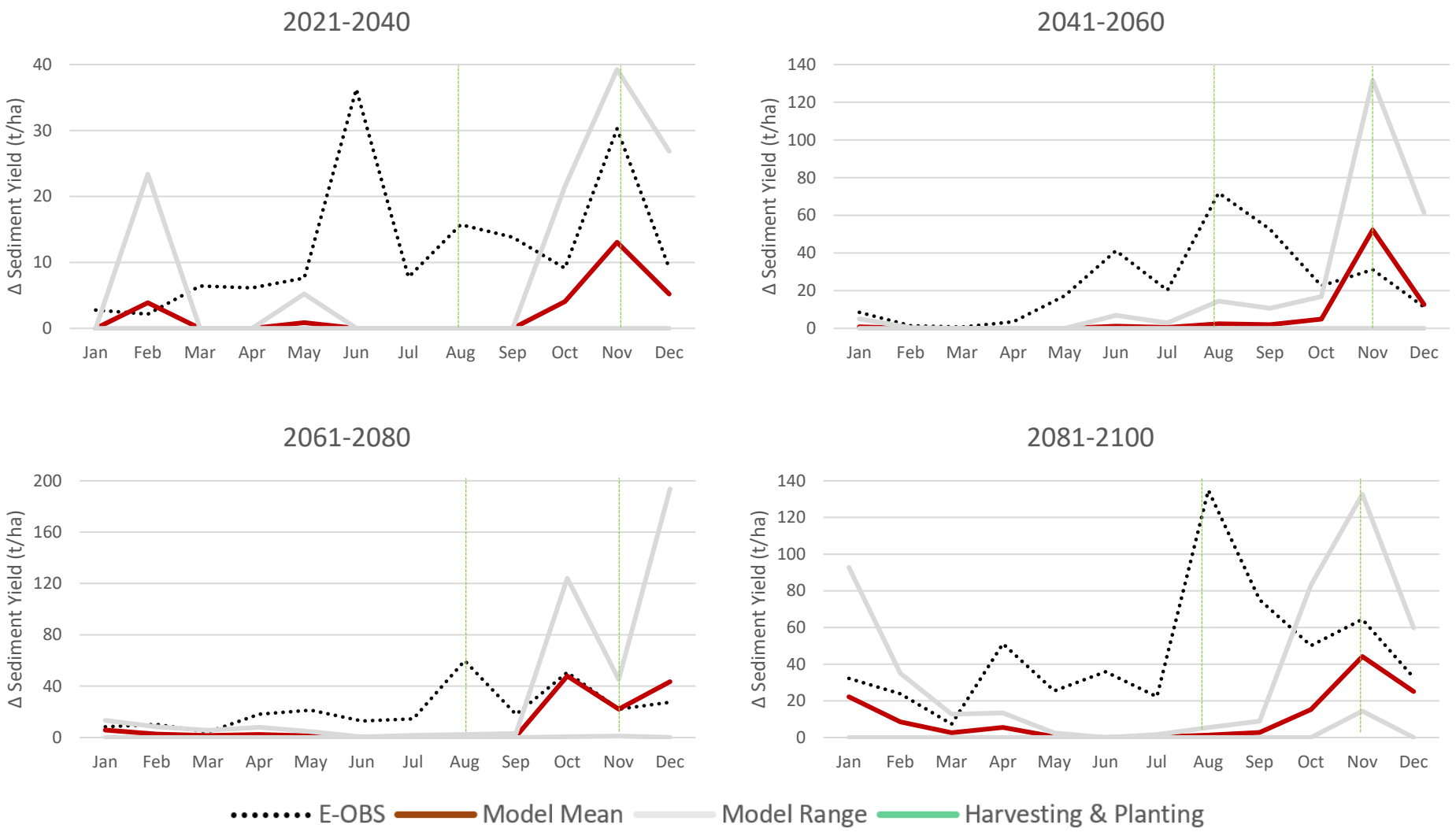

Figure 13: Seasonal changes in 'winter wheat only' mean modelled sediment yield (SY) in kg/m compared against the 'baseline' land use scenario between 2021-2100 for the GWW Hillslope. The model range is displayed for each month, while planting (November) and harvesting (August) dates are also indicated.

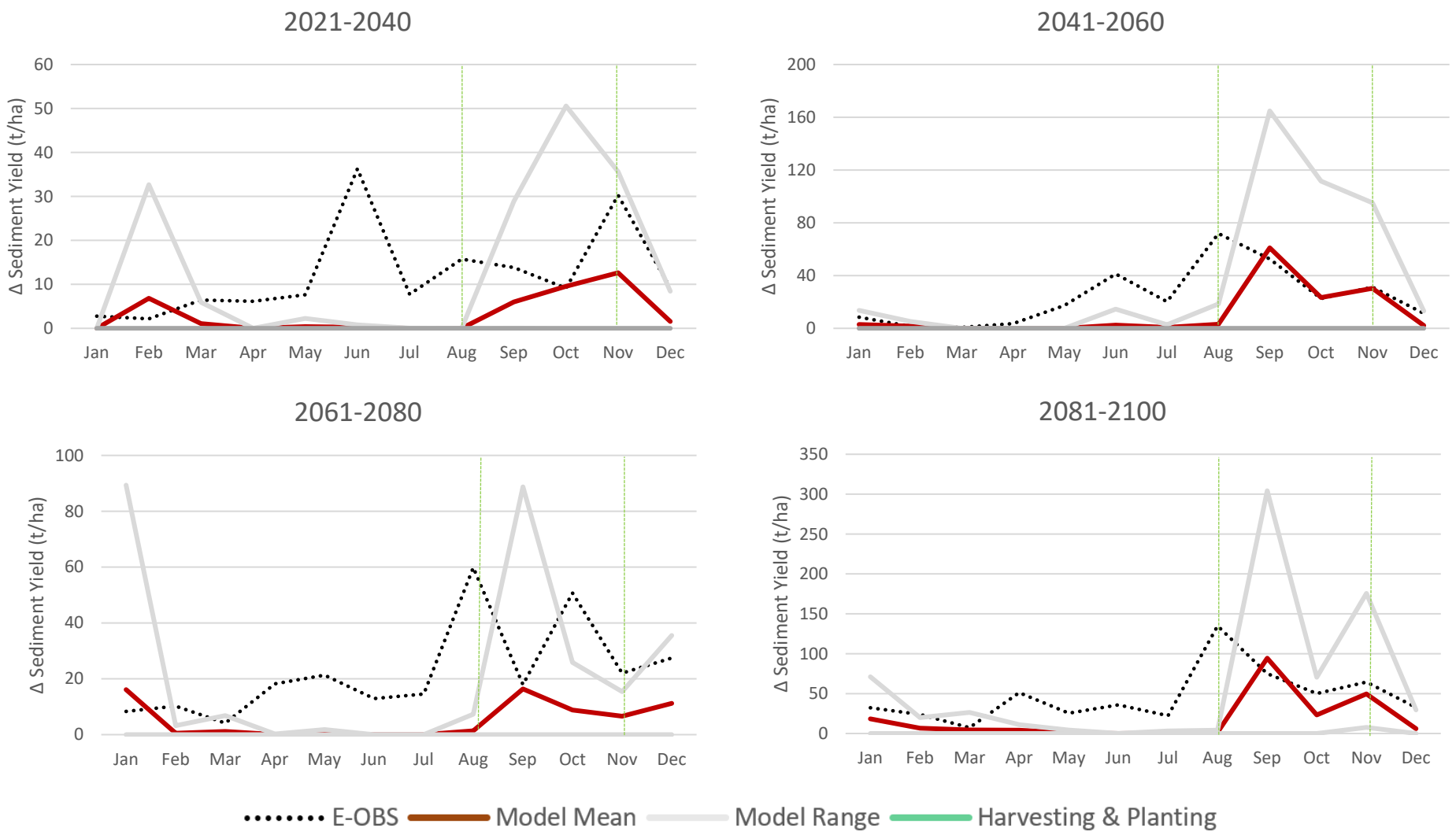

Figure 14: Same as for Figure 13, except for the 'winter wheat with cover crop' scenario for the GWW Hillslope. Tillage preparation and planting of the cover crop occurs in September.

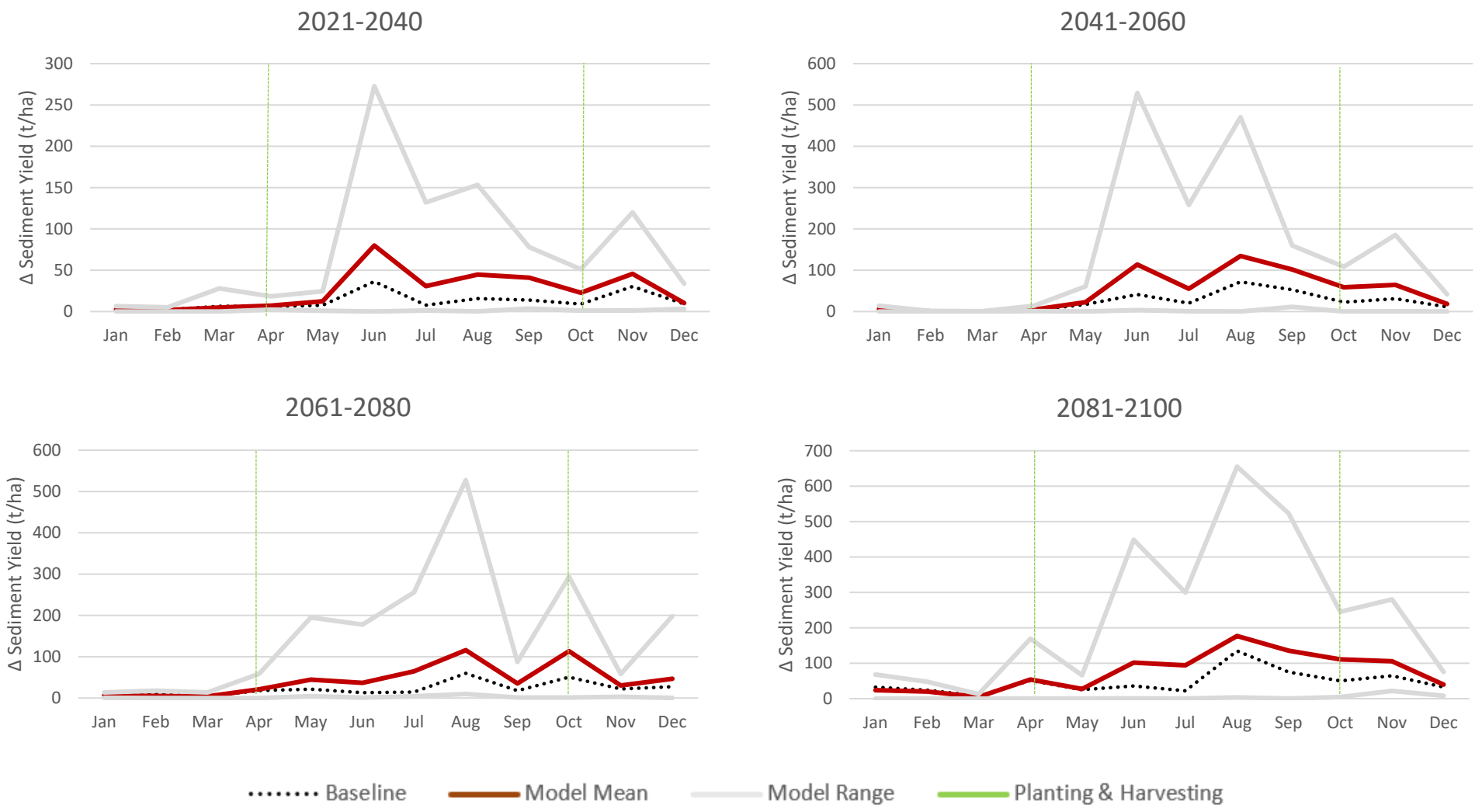

Figure 15: Same as for Figure 13, except for the 'summer crops only' scenario for the GWW Hillslope.

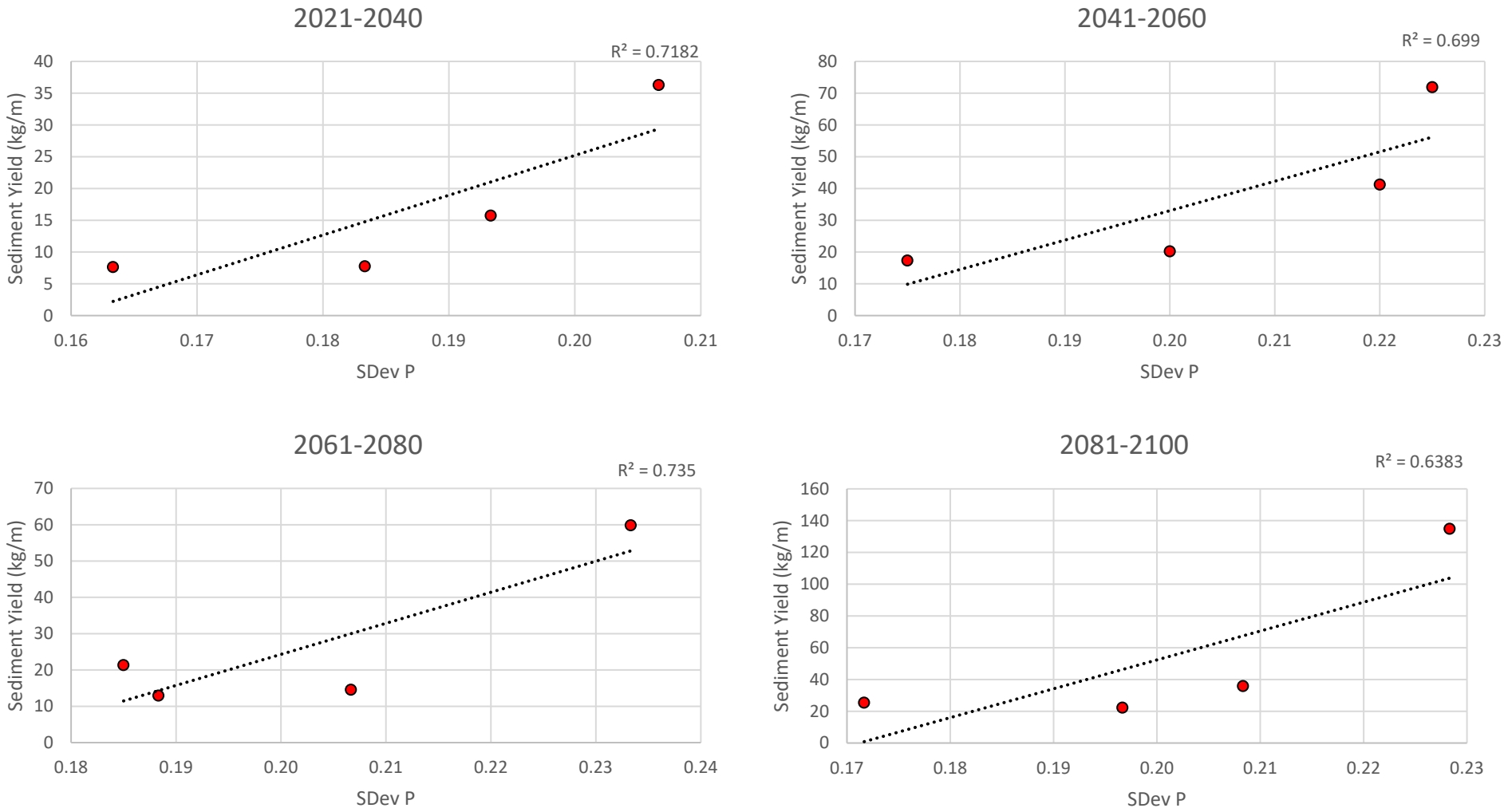

Figure 16: Correlation plots for sediment yield against SDEV P under current land management practices between 2021 and 2100 at the GWW Hillslope for May to August, which represent months of increased soil exposure.

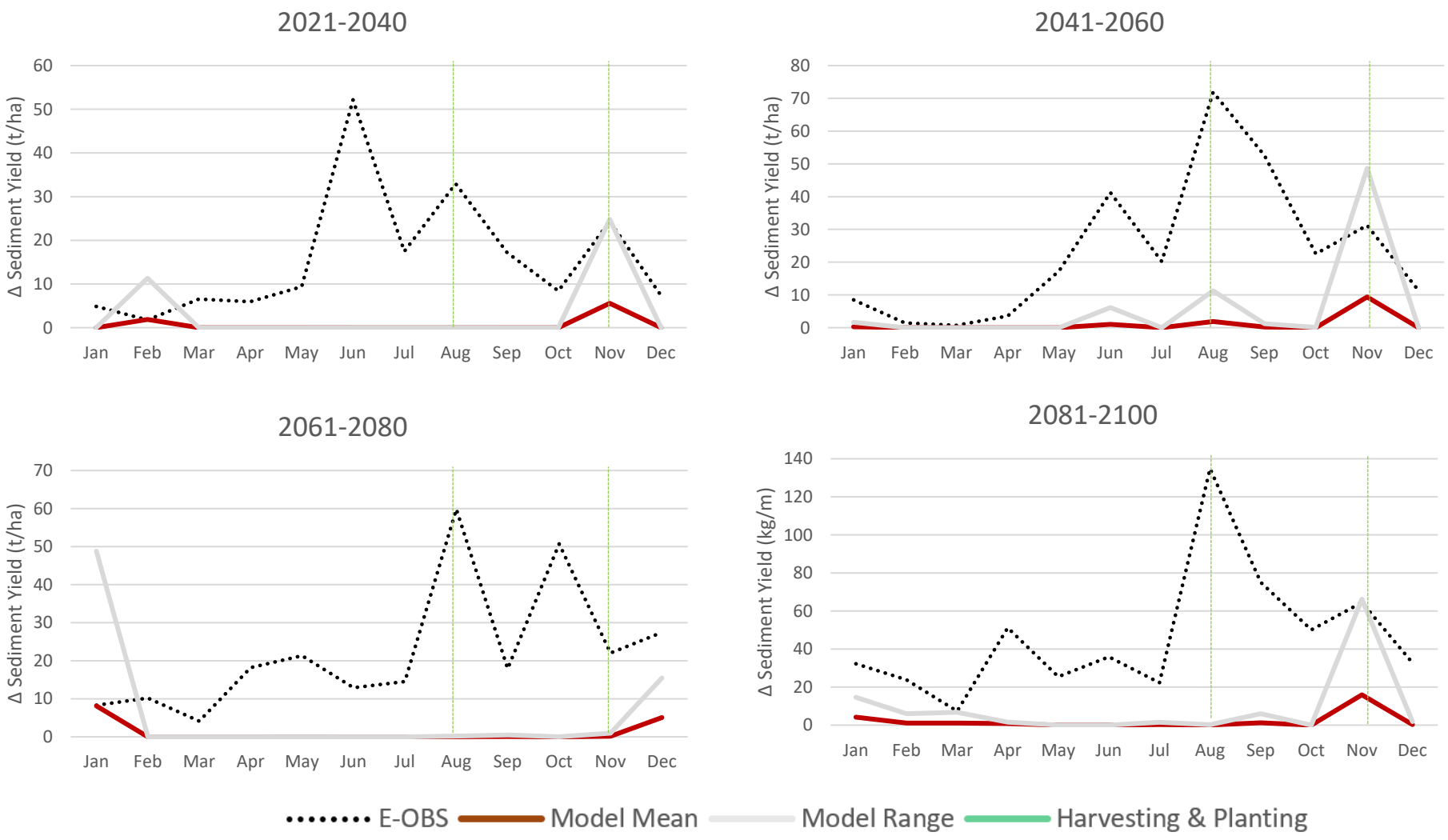

Figure 17: Same as for Figure 14, except cover crops are planted in September without tillage preparation at the GWW Hillslope

1